Contrib Mineral Petrol (2010) 159:541–561
DOI 10.1007/s00410-009-0441-2

ORIGINAL PAPER

Degassing, crystallization and eruption dynamics at Stromboli: trace element and lithium isotopic evidence from 2003 ashes

Federica Schiavi · Katsura Kobayashi · Takuya Moriguti · Eizo Nakamura · Massimo Pompilio · Massimo Tiepolo · Riccardo Vannucci

Received: 18 March 2009 / Accepted: 18 August 2009 / Published online: 3 September 2009

Abstract During its 1800-year-long persistent activity the Stromboli volcano has erupted a highly porphyritic (HP) volatile-poor scoriaceous magma and a low porphyritic (LP) volatile-rich pumiceous magma. The HP magma is erupted during normal Strombolian explosions and lava effusions, while the LP one is related to more energetic paroxysms. During the March–April 2003 explosive activity, Stromboli ejected two typologies of juvenile glassy ashes, namely highly vesicular LP shards and volatile-poor HP shards. Their textural and in situ chemical characteristics are used to unravel mutual relationships between HP and LP magmas, as well as magma dynamics within the shallow plumbing system. The mantle-normalized trace element patterns of both ash types show the typical arc-lava pattern; however, HP glasses possess incompatible element concentrations higher than LP glasses, along with Sr and Eu negative anomalies. HP shards are generally characterized by higher Li contents (to $\sim$20 ppm) and lower δ^7Li values (+1.2 to −3.8‰) with respect to LP shards (Li contents of 7–14 ppm and δ^7Li ranging between +4.6 and +0.9‰). Fractional crystallization models based on major and trace element compositions, combined with a degassing model based on open-system Rayleigh distillation and on the assumption that $^{melt/fluid}D_{Li} > 1$, show that abundant ($\sim$30%) plagioclase precipitation and variable degrees of degassing can lead the more primitive LP magma to evolve toward a differentiated (isotopically lighter) HP magma ponding in the upper conduit and undergoing slow continuous degassing-induced crystallization. This study also evidences that in March 2003 Stromboli volcano poured out a small early volume of LP magma that traveled slower within the conduit with respect to later and larger volumes of fast ascending LP magma erupted during the April 5 paroxysm. The different ascent rates and cooling rates of the two LP magma batches (i.e., pre- and post-paroxysm) resulted in small, but detectable, differences in their chemical signatures. Finally, this study highlights the high potential of in situ investigations of juvenile glassy ashes in petrologic and geochemical monitoring the volcanic activity and of Li isotopes as tracers of degassing processes within the shallow plumbing system.

Keywords Stromboli · Volcanic ash · Lithium isotopes · Degassing-induced crystallization · Petrologic monitoring

Communicated by J. Hoefs.

Electronic supplementary material The online version of this article (doi:10.1007/s00410-009-0441-2) contains supplementary material, which is available to authorized users.

F. Schiavi (✉)
Bayerisches Geoinstitut, Universität Bayreuth,
95440 Bayreuth, Germany
e-mail: Federica.Schiavi@uni-bayreuth.de

K. Kobayashi · T. Moriguti · E. Nakamura
The Pheasant Memorial Laboratory for Geochemistry and Cosmochemistry (PML), Institute for Study of the Earth's Interior, Okayama University at Misasa, Tottori-ken 682-0193, Japan

M. Pompilio
Istituto Nazionale di Geofisica e Vulcanologia, Sezione di Pisa, 56126 Pisa, Italy

M. Tiepolo · R. Vannucci
CNR, Istituto di Geoscienze e Georisorse, Sezione di Pavia, 27100 Pavia, Italy

R. Vannucci
Dipartimento di Scienze della Terra, Università degli Studi di Pavia, 27100 Pavia, Italy

Introduction

Magma batches ascending from sources to the surface through volcanic conduits undergo various processes at distinct depth levels, such as fractional crystallization, periodic magma recharging, magma mixing, interaction with older crystal mush, crustal contamination, and degassing. Magmatic processes taking place during magma ascent and storage at shallow levels may result in complex textural and compositional features of bulk rock samples, thus making the origin and the evolutionary path of the erupted magma difficult to be inferred. It is worth noting that a proper understanding of eruptive dynamics and magmatic processes that may occur within upper conduits is a crucial target in monitoring active volcanoes. Recent studies (e.g., Métrich and Rutherford 1998; Couch et al. 2003; Berlo et al. 2004; Blundy et al. 2006; Noguchi et al. 2006; Guilbaud et al. 2007; Piochi et al. 2008) stressed the importance of the interplay between degassing and crystallization and their link to eruptive style and magma ascent rate. Other studies (Wolf and Eichelberger 1997; Francalanci et al. 1999, 2005; Tepley et al. 2000; Landi et al. 2004) shed light on mechanisms of magma mixing between fresh reservoir-derived and conduit-resident magmatic components that can be genetically related or products of different sources. In these studies, different petrological and geochemical approaches were used to constrain changes in the physico-chemical condition of the magma during its storage and transit prior to or during eruption. Textural, compositional, and isotopic investigations of phenocryst assemblages, microlite groundmass and glassy matrix of pyroclasts, and lava samples provide insights into magmatic processes (e.g., Cashman 1992; Corsaro and Pompilio 2004; Landi et al. 2004; Schiavi et al. 2006; Guilbaud et al. 2007). Correlations between vesicles and microlite textures help understand the fluid mechanics of ascending magmas (e.g., Noguchi et al. 2006; Lautze and Houghton 2007). Combined studies of bulk rocks and phenocrysts-hosted melt inclusions help infer magma dynamics in active volcanoes (e.g., Métrich et al. 2005; Blundy et al. 2006).

At Stromboli volcano relationships between magmas that produce the highly vesicular, low-porphyritic pumices (hereafter LP magma) and those producing highly porphyritic, dark-colored scoriae (hereafter HP magma) erupted during its 1800-year-long persistent activity are at present a matter of debate that involves several disciplines (Bertagnini et al. 1999; Francalanci et al. 1999, 2004; Rosi et al. 2000; Métrich et al. 2005). Since these two magmas are strictly associated with dramatically different eruptive styles (HP is erupted during the normal Strombolian explosions and lava effusions, while LP is related to more energetic paroxysms), the understanding of their relationships would also contribute to improve monitoring strategies and assessment of volcanic hazards. Recent eruptions (2002–2003 and 2007) represent an excellent case study to unravel origin and significance, and mutual relationships between these two magmas, since a large volume ($>20 \times 10^6$ m^3) of HP magma was erupted as lava from subterminal vents in the Sciara del Fuoco, while LP magmas were poured out during the two largest paroxysms of the past 50 years (Métrich et al. 2005; Ripepe et al. 2005; Landi et al. 2006, 2009; Rosi et al. 2006). In addition, the multidisciplinary monitoring system that was activated few days after the beginning of the 2002–2003 eruptive crisis allowed more detailed volcanological observations accompanied by a systematic sampling of eruptive products and by more massive collection of geophysical and geochemical signals. These efforts improved significantly our capability of tracking magma dynamics within this volcano. The evolution of the reservoir that produced HP magma was monitored by systematic sampling and analysis of erupted lava (Landi et al. 2006, 2009), while the petrology of 2003 LP magma was studied by Métrich et al. (2005).

In this paper we focus on products erupted before and after the paroxysm that occurred on April 5, 2003, in order to track the magmatic processes that occur in response to changes in eruptive styles. We investigated both selected lava samples and pumices erupted during the paroxysm as representative of the main reservoir of HP magma and the uprising LP magma, respectively. Moreover, we put special emphasis on juvenile glassy ashes erupted from the summit craters before and after the paroxysm as proxy of processes that occur in the conduit just before and after large explosive events. A similar approach was successfully employed in several volcanoes to document the arrival of fresh magma at very shallow level (Watanabe et al. 1999; Cashman and Hoblitt 2004; Schiavi et al. 2006). We further combine information from trace elements and lithium isotopes to make inferences on geochemical signatures of magmas feeding the present-day activity and their variations as a consequence of crystal fractionation and degassing during the melt ascent to the surface, and syn- or post-emplacement processes (alteration, interaction with hot hydrothermal or magmatic fluids).

Lithium is a fluid-mobile element, moderately incompatible in magmatic processes (Ryan and Langmuir 1987; Brenan et al. 1998). Due to the large relative mass difference ($\sim$17%) between ^{6}Li and ^{7}Li, Li isotopes are largely fractionated in terrestrial systems, mainly at relatively low temperatures and during solid/fluid reactions (e.g., Chan et al. 1992, 2002a; James et al. 2003; Wunder et al. 2006, 2007). By virtue of its properties, lithium represents a potential geochemical tracer for a wide range of geological processes (see Tomascak 2004 for a review), such as

crust/mantle recycling at subduction zones and formation of mantle inhomogeneities (e.g., Moriguti and Nakamura 1998a; Chan et al. 2002b; Tomascak et al. 2002; Zack et al. 2003; Elliott et al. 2004, 2006; Leeman et al. 2004; Marschall et al. 2007; Halama et al. 2009), peridotite–melt interaction and peridotite metasomatism (e.g., Jeffcoate et al. 2007; Tang et al. 2007; Halama et al. 2009), and low-temperature alteration (e.g., Chan et al. 1992, 2002a; Rudnick et al. 2004; Teng et al. 2004). As for our purposes, fractionation of Li isotopes in juvenile glassy ashes relative to primary magma values may provide evidence about volatile exsolution, separation from the melt and outgassing, diffusion, and possible alteration or interaction with hot fluids after the emplacement.

Finally, in this paper we check the consistency of inferences on magma evolution and eruption dynamics of present Stromboli from chemical investigations of juvenile glassy ashes with evidence from studies of olivine-hosted melt inclusions, bulk rocks and mineral chemistry (Francalanci et al. 1999, 2004; Métrich et al. 2001; Bertagnini et al. 2003; Landi et al. 2006).

Recent Stromboli eruptive activity: a petrologic and volcanologic background

Stromboli is an active volcano placed on the convergent margin between the European and African plates. It belongs to the Aeolian arc, which is associated with recent subduction of the Ionian Plate as indicated by an active NW-dipping Benioff zone beneath the southern Tyrrhenian Sea (e.g., Gasparini et al. 1982). Stromboli has been erupting continuously with the present-day style for about 1800 years (Rosi et al. 2000), while its eruptive style between 6 and 2 ky is still poorly known (see discussion in Di Roberto et al. 2008 and Speranza et al. 2008). Its typical activity, known as "Strombolian activity", consists of mildly explosive jets, at variable intervals (~3–5 events per hour), of hot gas, scoriaceous bombs and lapilli, blocks, and ash from the summit crater vents interspersed by quiescent degassing with puffs and gas plumes. Effusive eruptions, as lava overflows from summit crater or fed by subterminal fissures, sometimes interrupt the normal activity (e.g., Landi et al. 2006, 2009). Sudden transition from the usual mild explosive activity to more violent, though short (few minutes), explosive phases (paroxysms) can also occur (Bertagnini et al. 1999, and references therein). Paroxysms largely vary as for style and size of products; these latter range from lapilli to meter-sized spatter or ballistic blocks and can be limited to the whole summit area or also blanket the lower flank of the edifice down to the inhabited areas (Speranza et al. 2004; Rosi et al. 2006).

Two magmas, shoshonitic to high-K basalts in composition, with sharply distinct physico-chemical characters are resident in the Stromboli plumbing system. They interact, mingle, and mix during ascent and eruption (e.g., Francalanci et al. 1999, 2004, 2005; Landi et al. 2004). The highly vesicular, low-porphyritic (phenocrysts <10 vol%) pumiceous magma (LP) is considered the primitive volatile-rich deep magma which feeds only paroxysms by rising very fast to the surface from a depth of 7.5–11 km, corresponding to a pressure range of 200–300 MPa (Bertagnini et al. 2008, and references therein). The dark-colored, scoriaceous magma (HP) represents a highly porphyritic (phenocrysts ~45–60 vol%), volatile-poor magma erupted by the normal Strombolian activity. The HP magma has been supposed to reside at shallow level, probably <3 km beneath the summit of the volcano, in a reservoir that in a steady state undergoes continuous erupting, crystallizing (plagioclase and minor olivine + clinopyroxene), and refilling by the deeper LP magma (Francalanci et al. 2004; Di Carlo et al. 2006; Landi et al. 2006). Assuming steady state conditions, Francalanci et al. (1999) estimated, on the basis of Sr isotope variations, relatively small (from 0.3 to 0.04 km^3) volumes and relatively long residence times (ca. 19 years) for HP magma residing in the shallow plumbing system. Burton et al. (2007) and Lautze and Houghton (2007) calculated from degassing models residence times of days or months in conduits (<250 m below summit).

Previous studies (Métrich et al. 2001; Bertagnini et al. 2003; Francalanci et al. 2004, 2005) showed that the LP magma has a less evolved composition (i.e., lower incompatible trace element contents) and higher volatile contents than the HP magma. Moreover, the two magma types show different mineral compositions. Both types of magma have kept rather constant major and trace element compositions in the last 1400–1800 years, which implies steady state conditions and no significant changes in mechanisms of differentiation. A small but significant difference between the LP and the HP magma has been observed also in terms of strontium isotope ratios ($^{87}Sr/^{86}Sr$ 0.70610 vs. 0.70625; Francalanci et al. 1999, 2005) only in products of recent years (after AD 1980), leading the authors to propose that the two kinds of magma have different sources. Regardless of possible different sources, Métrich et al. (2001) recognized within olivine-hosted melt inclusions the presence of primitive melts not yet identified as erupted magmas. These melts most likely represent the parent magma of LP pumices and shards. Métrich et al. (2001) proposed that the degassed crystal-rich magma results from the crystallization, driven by decompression and water loss, of volatile-rich LP magma batches which periodically ascend and refill the shallow part of a vertically elongated conduit (dike-like system) and partially mix with the crystal-rich body. Mingling and mixing

between LP and HP magmas has been interpreted as one of the main pre- and syn-eruptive processes that control petrography, textures, and zoning of phenocrysts and in general the magmatic evolution of Stromboli present-day products (Francalanci et al. 1999, 2004; Landi et al. 2004, 2006, 2008, 2009; Andronico et al. 2009).

The most important eruption in the past decades occurred between December 28, 2002, and July 22, 2003. This eruption had a complex evolution (see Landi et al. 2006) that comprised the following: (1) the onset of effusive eruption from a vent on the upper NE side of the Sciara del Fuoco, followed by a fast draining of the summit portion of conduits and cessation of the Strombolian activity, (2) the formation of landslides on the Sciara del Fuoco that caused a tsunami event, (3) the development of a 10^7 m^3 compound lava flow from a complex fissure system on the NW upper flank of the volcano, (4) the longest interruption of the summit Strombolian explosions in recent times (from the end of December 2002 to the beginning of May 2003), and (5) the strongest paroxysm of the last decades that ejected meter-sized blocks up Stromboli and Ginostra villages. It is noteworthy that, though Strombolian explosions were not visible before the paroxysm and until May, the location of very-long-period (VLP signals) seismicity, most likely produced by the ascent and associated rapid expansion of large gas slugs within the magma column, remained stable, confined to a zone of 250 m below the summit craters, before during and after the effusive eruption (Ripepe et al. 2005). In addition, repeated episodes of ash emissions and an inversion of the subsidence trend were observed since the beginning of March on the summit area as result of the progressive rise and accumulation of magma within the conduits (Puglisi et al. 2005). All the effusive products are HP (Landi et al. 2006), whereas HP and LP coexist sometimes deeply mingled even at the microscopic scale in the products of the April 5 paroxysm (Métrich et al. 2005).

Sampling and analytical methods

Sample description

The collected sample suite includes four pre-paroxysm ash samples that were erupted in March 2003 (STR08-03-2003, STR27-03-2003A, STR27-03-2003B, STR29-03-2003C) and two post-paroxysm ash samples that were ejected in April 2003 (STR10-04-2003A, STR10-04-2003B). The sample that was erupted on March 8 (STR08-03-2003) represents the first ash ejected from summit craters since the onset of effusive activity on December 28, 2002, and the first available for sampling. At the microscopic scale samples consist of various components (in order of abundance): blocky (grayish to reddish) lithic clasts, crystals (plagioclase, clinopyroxene and olivine), and glass shards. Among the glass shard components, amber to dark brown, poorly vesicular clasts are always found (Fig. 1a, c), but, interestingly, only two samples (STR08-03-2003 and

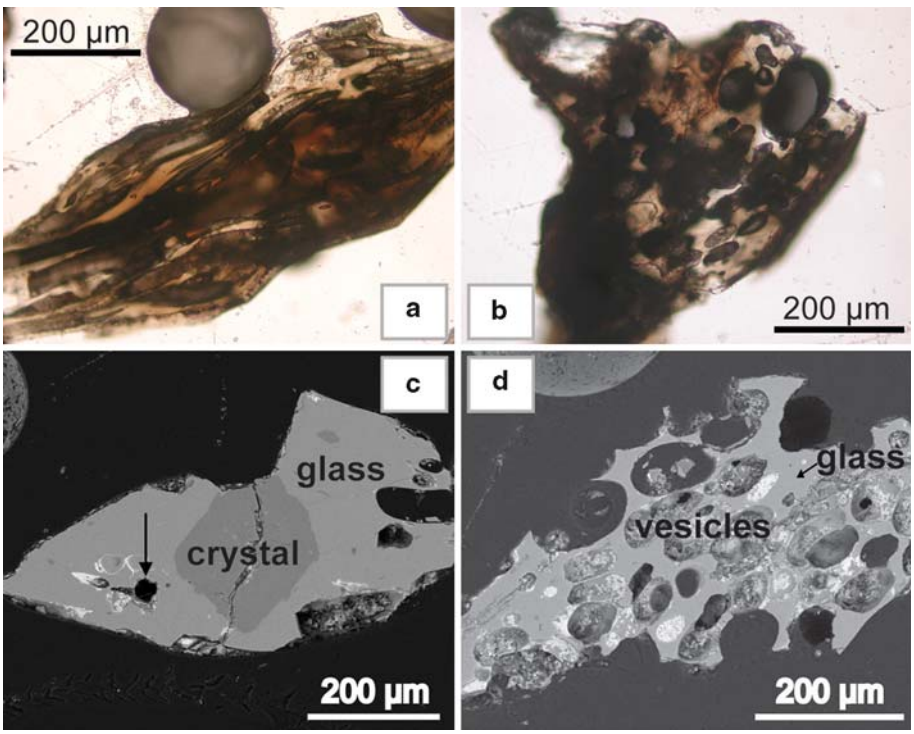

Fig. 1 Optical microscope and backscattered (BSE, Scanning electron microscope S-3100H, ISEI, Misasa, Japan) images of HP (**a–c**) and LP (**b–d**) glassy ashes. Crystals and vesicles are dispersed in the glassy matrix. One crater of trace element analyses by LA-ICPMS is indicated by the *arrow*

STR10-04-2003B) contain rare gray-yellow colored (light to transparent in thin section), strongly vesiculated, juvenile glassy fragments (Fig. 1b, d). By comparison with larger samples (lapilli and bombs) we consider the brown clasts as representative of HP magma (hereafter HP shards), whereas vesiculated and light-colored shards are associated with LP magma (hereafter LP shards). For the purpose of this work we selected about 50 and 10 fragments of 150–500 μm-sized glassy particles from HP and LP shards, respectively. Fragments with irregular and sharp outlines, low microlite content, and without alteration surfaces were preferred in order to avoid clasts that underwent recycling within the craters. HP shards contain nearly euhedral prismatic crystals (plagioclase, clinopyroxene and olivine), smaller than 250 μm in size (Fig. 1c), sometimes forming crystal clusters; on the contrary, no crystal was detected in LP shards. HP shards are characterized by lower degree of vesiculation in comparison to LP fragments (~10–40 vs. ~30–70 vol% vesicles as determined by optical microscope inspection). Mostly, vesicles embedded in HP shards are moderately elongated and, rarely, have sub-spherical shapes; stretched deformed bubbles are also present (Fig. 1a). LP shards contain smaller (<150 μm) but more numerous vesicles (Fig. 1b, d).

For comparison, chemical and isotopic investigations were conducted on seven whole-rock samples. Three samples belong to the 2003 volcanic activity, namely a LP pumice sample ejected during the April 5 paroxysm (ST317) and two lava samples (STR010203 and STR170503) erupted just before and after the paroxysm, respectively. The petrographic descriptions of these samples along with their major and trace element compositions are reported in Métrich et al. (2005) and Landi et al. (2006). Both pumice and lava samples strictly resemble compositions of whole-rocks erupted in the past decades (Fig. 2). The other samples were erupted during the "Recent Stromboli" activity period (<5.6 ± 3.3 ky BP; Gillot and Keller 1993; Hornig-Kjarsgaard et al. 1993) and include the pumices ST79p, ST81p and ST82p, and a lava sample from S. Bartolo (ST103). The pumice samples were collected from tephra layers in stratigraphic trenches dug on the NE flank of the volcano at about 450 m a.s.l. (Rosi et al. 2000). Their origin is related to paroxysmal eruptions that occurred after the third to seventh century AD (Rosi et al. 2000). Detailed studies of the mineralogy together with major and trace element geochemistry of these pumice samples were published by Métrich et al. (2001) and Bertagnini et al. (2003). The pumices belong to the high-K basalt field in the SiO_2–K_2O diagram of Peccerillo and Taylor (1976), and are analogous to LP pumices emitted in the twentieth and twenty-first centuries AD during paroxysms and major eruptions (Bertagnini et al. 2003, and Fig. 2). S. Bartolo lavas were erupted between 360 BC and 7 AD in Greek-Roman times from a parasitic vent NE of the present crater (Speranza et al. 2008). The petrography, mineralogy, and bulk-rock chemistry of S. Bartolo lavas are reported in Hornig-Kjarsgaard et al. (1993), Laiolo and Cigolini (2006) and Speranza et al. (2008). They consist of high-K calc-alkaline porphyritic basalts, and are among the less evolved lavas sampled on Stromboli Island (Fig. 2).

Micro-analytical techniques

Selected glass clasts were embedded in resin mounts and polished for quantitative geochemical analyses. The whole data set is reported in Tables 1 and 2. Major element composition of the glasses was determined by EMP at the CNR-IGG-Firenze (Italy) with a JEOL JXA-8600 (see Vaggelli et al. 1999 for analytical details), except for the samples STR08-03-2003 and STR10-04-2003B analyzed at the Bayerisches Geoinstitut (Bayreuth, Germany) using a JEOL JXA-8200 electron microprobe. The data were acquired with an accelerating voltage of 15 kV and a beam current of 15 nA. Counting times for glasses were 20 s on peak and 10 s on background. Trace element concentrations were measured by LA-ICPMS at the CNR-IGG-Pavia (Italy) using a 266-nm laser probe (Brilliant, Quantel; for further details, see Tiepolo et al. 2003) coupled with ICPMS (DRCe, PerkinElmer). The laser was operated at 10 Hz of repetition rate, the power on the sample was 1.5 mW, and spot size was set at 40 μm. The masses, representing the best compromise between maximum isotopic abundance and minimum presence of interference, were acquired in peak hopping mode with a dwell time of 10 ms. NIST SRM 610 and ^{44}Ca were adopted as external and internal standards, respectively. Precision and accuracy were evaluated on the USGS-BRC-2 reference material and are estimated to be better than 5 and 10% relative, respectively. Water contents on few glass fragments were determined by ion microprobe at the CNR-IGG-Pavia with a CAMECA ims-4f. Analytical details are reported in Ottolini et al. (1995).

Determination of Li isotope composition by ion probe was undertaken at the Pheasant Memorial Laboratory (PML) for Geochemistry and Cosmochemistry, Institute for Study of the Earth's Interior (ISEI), Okayama University at Misasa, Japan (Nakamura et al. 2003). Li isotope ratios were determined using a CAMECA ims-1270 ion probe with a multicollection system. Samples were polished and washed with diluted HF for 1 min, rinsed three times using Milli-Q water, then put in an ultrasonic bath with 0.5 M HNO_3 followed by Milli-Q water, for 5 and 3 min, respectively; subsequently they were dried and gold-coated for SIMS analysis. Samples were sputtered

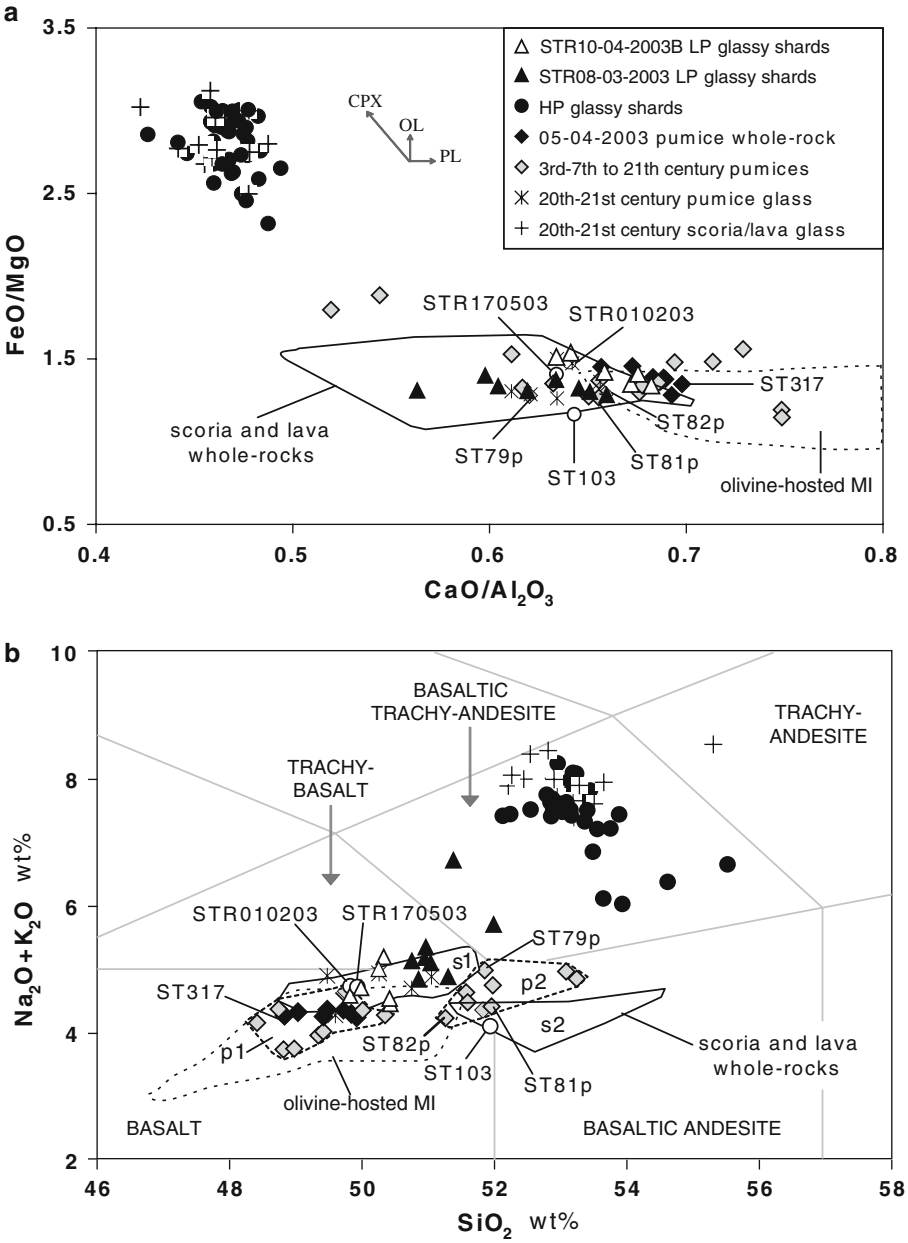

Fig. 2 CaO/Al_2O_3 versus FeO/MgO (**a**) and TAS classification scheme (**b**) for LP and HP glassy shards erupted in March–April 2003. Individual measurements are plotted. Bulk-rock compositions of pumices erupted in historical (third–seventh to twentieth century AD) and recent times (twentieth and twenty-first centuries AD; Rosi et al. 2000; Métrich et al. 2001; Bertagnini et al. 2003; Francalanci et al. 2004) and during the April 5, 2003, paroxysm (Métrich et al. 2005; Francalanci et al. 2008) are shown. The compositions of glassy matrix of recent pumices (Francalanci et al. 1999, 2004; Landi et al. 2004; Métrich et al. 2005) and recent scoriae, and lavas (Francalanci et al. 1999, 2004, 2008; Landi et al. 2004, 2006) are also plotted. Compositional fields for scoria and lava whole-rocks (Rosi et al. 2000; Métrich et al. 2001; Francalanci et al. 2004, 2008; Landi et al. 2004, 2006) and melt inclusions hosted in olivine phenocrysts of pumices (Métrich et al. 2001, 2005; Bertagnini et al. 2003) are reported. Labels refer to the whole-rock samples discussed in this work. **a** Vectors illustrate the effects of clinopyroxene, olivine, and plagioclase removal from melt. **b** Fields labeled with *p1* and *s1* include, respectively, pumices and scoriae/lavas from recent eruptions, whereas those labeled with *p2* and *s2* distinguish historical pumices from scoriae and lavas, respectively

with an O^- primary beam of 15 nA intensity resulting in pit diameters of ~20 μm, after ion sputtering. Secondary positive Li ions were accelerated at 10 kV and analyzed at a mass resolution of ~2,000. There are no ion interferences on target mass peaks at this mass resolution. The L2 and H2 electron multipliers were used for the collection of $^6Li^+$ and $^7Li^+$, respectively. Each analysis consisted of 55 cycles of 10 s counting of each cycle with 5 min of pre-sputtering. Before sample analyses, replicated analyses of synthetic basaltic glasses used as standards (see Kobayashi et al. 2004 for details) were measured in order to calculate the correction factor for the instrumental mass fractionation. The corrected isotopic ratios were expressed in per mil units:

$$\delta^7\mathrm{Li}(‰) = \left[\left(^7\mathrm{Li}/^6\mathrm{Li}\right)^{\mathrm{corr.}}_{\mathrm{SIMS}} \Big/ \left(^7\mathrm{Li}/^6\mathrm{Li}\right)_{\mathrm{ref}} - 1\right] \times 1{,}000$$

where NIST L-SVEC ($^7Li/^6Li = 12.119$) was used as reference value, as determined by TIMS, together with the measurements of standard glasses. The total analytical uncertainties (reported in Table 2) were calculated taking into account the internal precision of single measurements (±1.2‰, 2σ mean, on count rates of ~25,000 cps for $^7Li^+$), the reproducibility of measurements of standard

Table 1 Major and trace element average compositions of pre- and post-paroxysm HP and LP glassy shards

Sample STR	Pre-paroxysm HP shards								Post-paroxysm HP shards				Pre-paroxysm LP shards		Post-paroxysm LP shards	
	08-03-2003		27-03-2003A		27-03-2003B		29-03-2003C		10-04-2003A		10-04-2003B		08-03-2003		10-04-2003B	
	Average	SD (1σ)	Average	SD (1σ)	Average	SD (1σ)	Average	SD (1σ)	Average	SD (1σ)	Average	SD (1σ)	Average	SD (1σ)	Average	SD (1σ)
Number of analyses	10		5		7		4		6		8		8		6	
Major elements (wt.%)																
SiO_2	52.28	0.62	51.52	0.27	52.25	0.64	52.43	0.50	52.11	0.28	52.48	0.37	50.75	0.69	49.97	0.24
TiO_2	1.61	0.08	1.66	0.08	1.59	0.06	1.63	0.06	1.63	0.08	1.67	0.05	0.93	0.05	1.07	0.04
Al_2O_3	15.56	0.44	15.67	0.20	15.65	0.17	15.62	0.20	15.71	0.20	15.40	0.26	17.41	0.26	17.25	0.22
FeO	9.64	0.30	9.75	0.38	9.70	0.37	10.21	0.37	9.97	0.22	9.92	0.20	7.58	0.16	8.40	0.25
MnO	0.23	0.06	0.16	0.06	0.18	0.06	0.22	0.02	0.20	0.06	0.21	0.05	0.18	0.03	0.18	0.02
MgO	3.62	0.23	3.46	0.05	3.58	0.11	3.47	0.01	3.42	0.09	3.41	0.06	5.71	0.19	5.89	0.17
CaO	7.63	0.34	7.39	0.16	7.32	0.19	7.27	0.08	7.21	0.22	7.40	0.12	10.82	0.51	11.40	0.38
Na_2O	3.32	0.15	2.54	1.00	3.24	0.34	2.95	0.62	3.12	0.23	3.19	0.33	2.78	0.48	2.51	0.16
K_2O	4.19	0.10	4.31	0.10	4.08	0.24	4.01	0.56	4.22	0.20	4.34	0.04	2.55	0.20	2.22	0.14
P_2O_5	1.20	0.06	n.d.		n.d.		n.d.		n.d.		1.20	0.05	0.67	0.05	0.65	0.05
H_2O[a]	0.26												0.23		0.28	0.00
	Average	SD (1σ)	Average	SD (1σ)	Average	SD (1σ)	Average[b]	SD (1σ)	Average	SD (1σ)	Average	SD (1σ)	Average	SD (1σ)	Average[c]	SD (1σ)
Number of analyses	7		8		12		6		8		6		3		2	
Trace elements (ppm)																
Li	17.8	3.5	14.3	4.0	15.9	3.6	15.6	1.7	15.8	3.5	16.2	0.8	11.3	3.3	8.2	0.9
B	66.3	23.8	51.3	6.2	67.9	21.4	49.1	7.0	57.1	7.9	57.6	7.5	33.5	4.8	25.0	3.3
Sc	22.9	2.5	24.7	1.3	22.7	1.8	23.5	1.0	23.7	1.8	24.3	0.8	25.5	3.0	27.7	1.0
V	375	36	356	16	377	19	358	18	364	14	372	18	266	18	255	1
Cr	13.8	8.1	5.82	2.22	10.2	5.4	6.87	1.56	7.46	4.28	5.87	1.10	36.5	3.8	16.6	3.4
Co	25.1	3.6	23.6	1.3	23.6	1.5	23.2	2.2	23.3	1.3	24.6	1.0	29.7	2.8	31.4	0.2
Ni	13.4	6.1	10.0	1.3	11.0	3.0	8.65	1.77	8.81	0.81	10.6	1.5	43.3	8.3	33.0	1.3
Zn	101	29	83.1	11.3	82.3	8.7	92.7	8.8	87.5	17.2	108	25	84.0	12.8	77.9	7.1
Rb	171	51	141	12	147	14	139	11	143	3	151	10	84.3	8.4	64.9	2.2
Sr	645	48	577	17	592	58	561	5	563	15	560	12	873	20	675	11
Y	41.6	5.6	47.4	2.7	43.4	2.8	45.3	1.9	45.4	2.7	45.2	1.4	25.4	4.1	23.3	0.7
Zr	320	39	359	19	330	21	340	13	352	17	347	14	182	17	147	1
Nb	46.3	5.4	47.4	2.4	44.6	3.3	46.8	3.1	46.3	1.7	48.1	3.4	28.3	2.0	19.7	0.1
Cs	13.6	10.9	9.34	0.82	9.63	0.95	8.76	0.80	9.67	0.41	9.81	0.70	5.29	0.46	4.01	0.02
Ba	1663	130	1580	59	1635	114	1504	91	1642	62	1638	83	1189	74	853	12

Table 1 continued

	Average	SD (1σ)	Average	SD (1σ)	Average	SD (1σ)	Average[b]	SD (1σ)	Average	SD (1σ)	Average	SD (1σ)	Average	SD (1σ)	Average[c]	SD (1σ)
La	85.3	8.0	91.6	3.5	86.4	5.6	87.3	2.9	90.1	4.0	88.8	4.7	54.8	2.3	39.5	1.0
Ce	157	15	171	6	163	10	166	5	174	7	172	9	105	4	81.9	1.2
Pr	18.9	1.9	20.8	1.0	20.3	1.0	19.8	1.0	20.0	0.8	20.4	1.2	13.4	1.1	10.1	0.4
Nd	75.2	7.6	82.5	2.8	76.3	6.8	75.0	2.1	79.4	4.2	78.7	3.0	49.0	1.4	39.3	1.6
Sm	13.9	1.7	15.3	0.6	15.0	1.3	14.7	1.0	14.8	0.8	14.7	1.4	9.20	0.6	7.49	0.63
Eu	3.17	0.41	3.35	0.19	3.28	0.22	3.07	0.43	3.00	0.27	3.24	0.24	2.67	0.51	2.19	0.01
Gd	10.3	1.4	12.6	0.5	11.3	1.1	10.7	2.4	11.7	0.9	11.7	0.6	5.90	1.28	5.49	0.28
Tb	1.32	0.27	1.51	0.18	1.49	0.08	1.37	0.14	1.58	0.30	1.39	0.07	0.86	0.10	0.74	0.03
Dy	8.21	1.49	9.40	0.45	8.15	0.93	8.73	0.99	8.44	0.75	8.40	0.81	5.31	0.64	4.50	0.37
Ho	1.41	0.22	1.81	0.17	1.66	0.16	1.67	0.19	1.64	0.27	1.73	0.06	0.96	0.05	0.90	0.10
Er	4.33	0.63	4.80	0.56	4.19	0.45	4.57	0.58	4.18	0.95	4.44	0.47	2.56	0.75	1.90	0.45
Tm	0.590	0.088	0.646	0.082	0.557	0.105	0.560	0.079	0.634	0.089	0.585	0.073	0.234	0.085	0.338	0.052
Yb	4.17	0.92	4.56	0.53	4.05	0.51	3.57	0.78	4.27	0.58	4.42	0.63	1.96	0.32	2.04	0.45
Lu	0.599	0.191	0.678	0.101	0.633	0.079	0.617	0.087	0.548	0.120	0.624	0.069	0.296	0.026	0.268	0.017
Hf	7.05	1.19	7.87	0.62	7.33	0.47	7.41	0.78	7.41	0.86	7.44	0.48	4.37	0.28	3.22	0.18
Ta	2.26	0.35	2.60	0.14	2.25	0.17	2.55	0.23	2.80	0.56	2.51	0.16	1.17	0.24	1.00	0.15
Pb	48.8	23.9	33.0	3.5	34.1	5.3	31.6	2.6	31.2	2.7	34.2	2.3	38.0	21.6	18.7	2.4
Th	31.0	3.5	34.4	1.9	31.7	2.6	32.1	1.6	33.4	2.0	33.0	2.0	18.6	1.6	12.4	1.2
U	8.07	1.42	7.77	0.57	7.99	0.81	7.61	0.38	7.82	0.88	7.96	0.64	4.77	0.37	3.12	0.17

n.d. Not determined

[a] H_2O contents of STR08-03-2003 HP and LP shards represent single analyses, while H_2O content of STR10-04-2003 LP sample is average value of two analyses

[b] For Li, average of three analyses

[c] For Li and B, average of four analyses

Table 2 Li concentrations and Li isotopic compositions of HP and LP glassy shards and whole-rock samples

Sample	δ^7Li (‰)	Li (ppm)
HP glassy shards		
STR08-03-2003		
Fragment 1	+1.2 ± 0.8	14.1
Fragment 11	−2.4 ± 0.7	14.4
Fragment 10	−3.4 ± 0.6	15.3
Fragment 14	−3.8 ± 0.7	17.7
STR10-04-2003B		
Fragment 7	−2.9 ± 0.5	16.7
Fragment 19	−1.0 ± 0.4	15.3
Fragment 29	−0.4 ± 0.5	15.8
LP glassy shards		
STR08-03-2003		
Fragment 7	+4.6 ± 0.8	14.3
Fragment 8	+1.6 ± 0.8	7.8
Fragment 20	+0.9 ± 0.7	11.9
STR10-04-2003B		
Fragment 17	+4.2 ± 0.6	8.8
Fragment 12	+4.4 ± 0.7	7.3
Whole-rock lavas and pumices		
ST103	+3.12 ± 0.03	8.59
ST79p	+3.14 ± 0.03	10.12
ST81p	+3.49 ± 0.03	9.36
ST82p	+3.27 ± 0.03	8.83
ST317	+2.91 ± 0.10	8.21
ST010203	+3.58 ± 0.09	9.41
ST170503	+3.72 ± 0.08	9.21

glasses (< ± 4.8‰, 2σ), and the uncertainty related to the accuracy of the correction factor (~4‰; for further details about the analytical procedures, see Kobayashi et al. 2004).

Lithium isotope bulk-rock analysis

The lithium contents of bulk samples were measured prior to Li chemical separation to determine the required amount of sample material for Li isotope analysis. 20 mg of powder samples was digested in mixed acids [30 M HF, 7 M $HClO_4$, 16 M HNO_3, and 6 M HCl; the digestion method is described by Yokoyama et al. (1999)] to measure Li contents and isotope ratios (Table 2). Li was analyzed by ICP-MS (Agilent 7500cs housed at the PML, Okayama University at Misasa) following the procedures of Makishima and Nakamura (2006). The analytical error was typically less than 3% (2σ). Based on the Li content of each sample, appropriate aliquots of sample solution were used for lithium chemical separation, as described in Moriguti and Nakamura (1998b). The resulting Li fraction after column chemistry was dissolved in 0.5 M HNO_3 to produce a 10-ppb Li solution that has been analyzed for Li isotopes by MC–ICP–MS (Thermo-Finnigan Neptune, housed at the PML, Okayama University at Misasa). To obtain normalized isotopic compositions, sample analyses were bracketed by analyses of NIST L-SVEC standards (Tomascak et al. 1999a). In-run precision for analyses of standards and samples of this study was less than 0.06‰ (2σ mean); the relative difference in Li isotope ratios of the two standards bracketing each sample was typically less than 0.4‰. Further details including the instrumental setup and the operating conditions are reported in Tang et al. (2007). Analyses of nine separate digestions of the GSJ JB-3 standard rock sample performed in this study yielded a value of +4.63 ± 0.19‰ (2σ), in agreement with the values obtained by TIMS within the analytical error (+3.9 ± 0.7‰, 2σ reproducibility; Moriguti and Nakamura 1998b).

Results

Major element composition

On the basis of the different chemical compositions of glasses two kinds of shards can be distinguished. LP glassy shards are characterized by higher Al_2O_3, MgO, and CaO contents and CaO/Al_2O_3 ratios, and lower SiO_2, TiO_2, FeO, Na_2O, K_2O, and P_2O_5 contents in comparison to HP glassy shards (Fig. 2). In the total-alkali-silica (TAS) classification scheme, glasses of LP shards plot on the boundary between basalt and trachybasalt fields, apart from two fragments from the STR08-03-2003 sample with basaltic-trachyandesite compositions, whereas glasses in HP shards show basaltic-trachyandesite compositions (Fig. 2b). According to the SiO_2–K_2O classification diagram (Peccerillo and Taylor 1976) LP and HP shards have high-K calcalkaline-shoshonitic (K_2O = 2–3 wt.%) and shoshonitic (K_2O = 4–5 wt.%) signatures, respectively. LP shards erupted on April 10 (post-paroxysm) have higher FeO and TiO_2 contents and CaO/Al_2O_3 mean ratio and lower SiO_2, and alkali mean contents than the pre-paroxysm LP shards. Major element compositions of the analyzed HP and LP shards resemble those of the glassy matrix from HP scoriae and LP pumices (Francalanci et al. 1999, 2004, 2008; Landi et al. 2004, 2006, 2008), respectively (Fig. 2). If compared to April 5 pumice whole-rocks, the post-paroxysm LP shards show similar compositions with slightly higher mean SiO_2 and alkali contents and a lower CaO/Al_2O_3 mean value. Water content in HP and LP glasses is low (0.23–0.28 wt.%), with no significant difference between the two glass types. Similar H_2O contents (nearly 0.2 wt.%) characterize melt inclusions in minerals belonging to the HP magma (Métrich et al. 2001).

Trace element composition

Differences between the compositions of HP and LP shards are apparent as for the trace element signatures. As a whole, the mantle-normalized trace element patterns show the typical arc-lava pattern with enrichments in LILE, B, Pb, U, Th, and LREE relative to HFSE and HREE (Fig. 3). HP glasses erupted during the four investigated ash emission events are quite homogeneous and possess incompatible element concentrations higher than LP glasses. Moreover, HP glass shows Sr and Eu ($(Eu/Eu^*)_N = Eu_N/(Sm_N \times Gd_N)^{0.5} = 0.6–0.9$) negative anomalies, and slightly lower Ba/Rb ratios with respect to the LP glass. Concerning compatible elements, Cr, Ni, Co, and Sc contents decrease, whereas V content increases, from the LP to the HP glass. If compared with the post-paroxysm LP shards (STR10-04-2003B), the pre-paroxysm ones (STR08-03-2003) display a parallel compositional pattern, with slightly higher contents in all incompatible elements, but Yb. Cr, Ni, and V contents increase from the post-paroxysm to the pre-paroxysm LP glasses, while Sc and Co contents slightly decrease. The incompatible trace element pattern of post-paroxysm LP shards is coincident with those of pumice whole-rocks erupted in the twentieth century AD and during the April 5, 2003, paroxysm (Fig. 3). Pre-paroxysm LP shards closely resemble the glassy matrix of LP pumices and olivine-hosted melt inclusions embedded in the pumice ST82p (Schiavi 2007). HP glass shards differ from LP pumices for the higher trace element concentrations and the Sr negative anomaly.

For all samples taken together Cs, Rb, Ba, Th, U, LREE, MREE, and Ti draw positive correlations with SiO_2 contents (Fig. 4). Noticeably, whereas the content of most trace elements is homogeneous in HP shards (RSD $\approx$ 5% for LREE, Y, Nb and Zr; 5–10% for LILE, Ta, Hf, Th, U, and Pb; 10–12% for HREE), that of B and Li is more variable (RSD $\geq$ 20%). Lithium content varies from 6.5 up to 24 ppm and is weakly positively correlated ($R^2 \sim 0.5$) with Na_2O and B abundances (not shown).

Lithium isotopic signature

Li isotopes ratios of the pre-paroxysm and post-paroxysm HP shards show a significant variation from -3.8 ± 0.7‰ to $+1.2 \pm 0.8$‰. Post-paroxysm LP shards are homogeneous with an average composition of $\delta^7Li = +4.3 \pm 0.3$‰ ($2\sigma$), which resembles the δ^7Li signature of whole-rock pumice and lava samples analyzed by bulk method in this work (average value of $+3.3 \pm 0.6$‰, 2σ). δ^7Li of pre-paroxysm LP glass shards varies between $+0.9 \pm 0.7$‰ and $+4.6 \pm 0.8$‰; this range partially overlaps that of known values (-1.7 ± 0.9‰ to 2.3 ± 0.7‰) for olivine-hosted melt inclusions found in the pumices ST79p and ST82p erupted after the third and seventh centuries AD (Schiavi 2007).

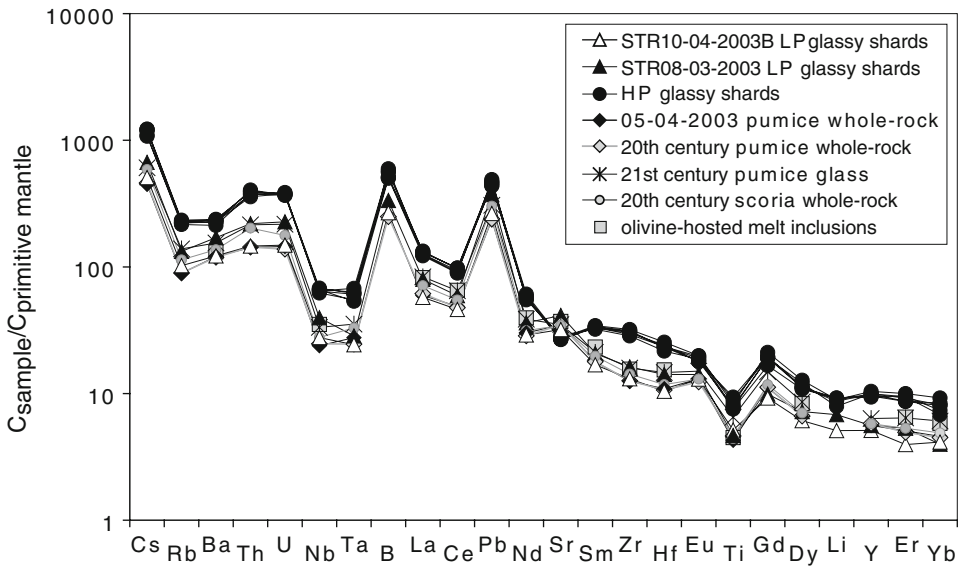

Fig. 3 Incompatible trace element compositions, normalized to primitive mantle (Sun and McDonough 1989), for HP and LP glassy shards erupted in March–April 2003. Trace element patterns of the average compositions of pumices erupted during the April 5 paroxysm (Métrich et al. 2005; Francalanci et al. 2008), pumices (Francalanci et al. 1999, 2004; Métrich et al. 2001; Bertagnini et al. 2003) and scoriae (Francalanci et al. 1999, 2004, 2008; Métrich et al. 2001) erupted during the twentieth century AD, and glassy matrix of twenty-first century pumices (Pompilio, unpublished data) are shown. Trace element composition of olivine-hosted melt inclusions embedded in the pumice ST82p (Schiavi 2007) is reported for comparison

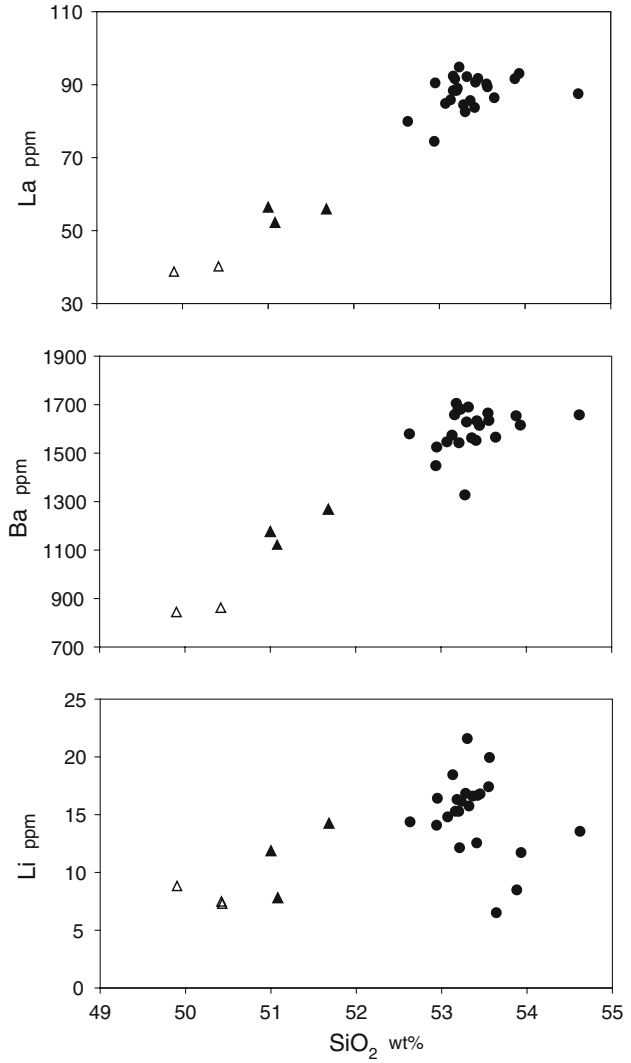

Fig. 4 Variation of representative incompatible trace elements relative to the SiO_2 content. An overall increase from LP to HP shards is observed. *Symbols* as in Fig. 2

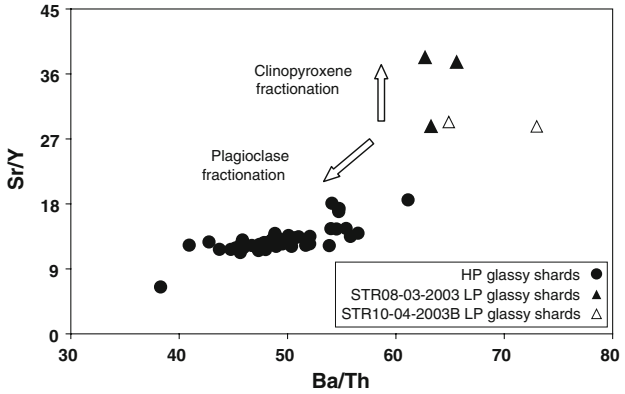

Fig. 5 Ba/Th versus Sr/Y plot, showing the differentiation trends of LP and HP ash glasses associated with dominant clinopyroxene or plagioclase fractionation

Discussion

Genetic relationships between LP and HP magmas

Previous studies of bulk-rocks and melt inclusions (Francalanci et al. 1999, 2004; Métrich et al. 2001; Bertagnini et al. 2003) suggested that different residence times within the plumbing system, associated with different rates of gas loss and crystallization en route, can explain the main differences in major and trace element composition between LP and HP magmas. Also the major and trace element fingerprinting of glassy ashes erupted by the explosive events in March–April 2003 confirms that HP shards represent, relative to LP analogs, a more evolved melt that underwent higher crystal fractionation degrees in the shallowest part of the conduit. Major evidence in favor of this comes from Sr and Eu negative anomalies that characterize HP shards and can be reconciled with the role of plagioclase as fractionating mineral (Figs. 3, 5). Fractional crystallization models based on major and trace element composition were used to test the origin of the more evolved component (HP glasses) from the more primitive one (LP glasses). For modeling, major element compositions of crystals, namely clinopyroxene, plagioclase and olivine recovered from the selected HP ash samples were used (eTable 1 in the Online Resource). Olivine (Fo70) and plagioclase (An65-An77) compositions overlap those of phenocrysts found in scoria samples erupted during the twentieth and twenty-first centuries AD (Francalanci et al. 2004; Landi et al. 2004). Analyzed clinopyroxene crystals in HP shards reveal augitic composition and Mg# [mol $Mg^{2+}/(Mg^{2+} + Fe^{2+})$] ranging between 0.75 and 0.78, although diopsidic compositions (Mg# $\sim$0.87), which provide evidence for resorption and/or assimilation processes, are also observed (e.g., STR10-04-2003A). Francalanci et al. (2004) and Landi et al. (2004) performed systematic studies on mineral chemistry and textural zoning of phases crystallized from scoriaceous and pumiceous magmas at Stromboli. These authors evidenced that mineral phases in equilibrium with the LP and HP magmas have distinct compositions. Fo% in olivine around 70, Mg# in clinopyroxene around 0.75, and An% in plagioclase around 65 are in equilibrium with the HP magma, whereas Fo% in olivine $\sim$80–85, Mg# in clinopyroxene $\sim$0.83–0.91, and An% in plagioclase $\sim$80–90 are in equilibrium with the LP magma (Francalanci et al. 2004). Francalanci et al. (2004) and Landi et al. (2004) also pointed out that successive intrusions of volatile-rich LP magma blobs at shallow depth and syn-eruptive mingling process between HP and LP magmas are responsible for partial crystal dissolution and complex phenocryst zoning. For the major element modeling only analyses of crystals

with compositions close to equilibrium with HP magma were used, in order to investigate the role of mineral fractionation at shallow depth. Major and trace element modeling was performed by mass balance calculation and by using the equation for fractional crystallization $C_{evolved}/C_{starting} = F^{D-1}$ (see explanation in the table caption), respectively. Phase proportions and total percentage of fractional crystallization were calculated to best fit the measured composition of the evolved melt (HP shards) by using the Microsoft Excel solver function. The results of the quantitative calculations are reported in detail in eTable 2 and eTable 3 (Online Resource). As a whole, major and trace element data from this work are consistent with an origin of HP glass from LP glass by 49–57% (best-fit for major and trace element modeling, respectively) fractional crystallization of a mineral assemblage consisting of prevailing plagioclase (27–33%) and minor clinopyroxene (16–18%), and olivine (4–6%), i.e., the phenocryst paragenesis of Stromboli magmas (e.g., Francalanci et al. 1999, 2004; Métrich et al. 2001; Landi et al. 2004). Our calculations show that the model fits well for almost all elements (eFig. 1 in the Online Resource). Small discrepancies in FeO and TiO_2 contents between the measured and calculated HP compositions are significantly reduced when Fe- and Ti–rich outer rims of clinopyroxene phenocrysts from scoria samples (Francalanci et al. 2004) are considered for modeling (eTable 2, Model 2). In evaluating the goodness of the fit, uncertainties due to the assumption of average compositions of glassy shards and mineral phases and uncertainties associated with mineral-melt partitioning coefficients of trace elements must be taken in consideration.

LP glasses: pre- versus post-paroxysm products

Textural (high vesicularity, absence of abrasion), petrographic (lack of alteration or palagonitisation), and geochemical (e.g., no anomalous compositions) characteristics of LP clasts erupted before the paroxysm all point to a juvenile nature and let to exclude processes of recycling of relatively old ash clasts residing within the crater. In fact even in a partially or momentarily obstructed crater of an active volcano, kinetics of alteration processes is very fast due to the high temperatures (>700°C according to Allard et al. 2008) and diffuse emission of gases. Exposures of basaltic glasses within the Etna crater allowed Spadaro et al. (2002) to demonstrate that morphological and chemical transformations of the clast surface occur in a very short time and become significant within a few hours. Above results are fully confirmed by some pilot experiments carried out at INGV-Pisa lab, in which a LP ash was kept at high temperature (>700°C) in a tube furnace. About 12 h of exposure at 750°C in oxidizing conditions ($fO_2 \sim$ atmospheric) produces the complete reddening of clast surfaces. Less oxidizing conditions ($fO_2 \sim$ NNO buffer) result in observable surface modifications and precipitation of very small secondary crystals, giving a gray dull appearance to the clast surface.

To the best of our knowledge, this is the first finding in Stromboli of LP clasts not erupted during a paroxysmal eruption. Small differences in major element compositions between pre-paroxysm and post-paroxysm shards, along with slightly higher abundances of incompatible trace elements, Cr, Ni, and V in the pre-paroxysm glasses are observed. The absence of negative Sr anomaly in LP shards rules out a significant role of plagioclase fractionation and suggests that both pre- and post-paroxysm LP glasses represent more primitive melts that ascended along the crust without stalling in shallow part of the plumbing system ($P < 50$ MPa), where plagioclase crystallization starts to occur in response of water loss due to degassing ($H_2O < 2.5$ wt.%; Di Carlo et al. 2006). Compositional variations between pre-paroxysm and post-paroxysm shards are therefore related to differentiation mechanisms occurring at depth. In this regard, it is worth noting that the incompatible trace element contents of the pre-paroxysm LP magma resemble those of olivine-hosted melt inclusions found in the pumice ST82p. Métrich et al. (2001) and Bertagnini et al. (2003) evidenced that these melt inclusions were not significantly affected by post-entrapment evolution and calculated entrapment pressures of ~300–400 MPa. Variable extents of crystal fractionation between LP magma batches were invoked by Métrich et al. (2001) to explain the mineralogy and chemistry of olivine-hosted melt inclusions from the pumiceous magma. Analogously, limited fractionation of mafic phases is likely to be responsible for higher abundances of incompatible trace elements observed in the pre-paroxysm LP glasses. However, such a simple process cannot explain the higher contents of Cr, Ni, and V observed in the pre-paroxysm glassy shards. The behavior of more compatible elements points to some assimilation of cumulates from fossil reservoirs or crystal mushes from the present-day reservoir during the interaction between basaltic melts and wall-rocks (e.g., Francalanci et al. 1989, 2005; Bertagnini et al. 2003; Pichavant et al. 2009). Application of pure AFC or energy-constrained AFC models is hampered by a number of factors including: (1) the chemical variability, systematic reverse zoning, and resorption textures shown by olivine and clinopyroxene (Francalanci et al. 2008); (2) the chemistry of mafic cumulates (e.g., Laiolo and Cigolini 2006), and (3) the adopted $^{Min/Liq}D$ values. In spite of these limitations, simple AFC models (eTable 4 in the Online Resource) indicate that Cr, Ni, and V contents are roughly consistent with fractional crystallization (~20%) of clinopyroxene (90%) and olivine (10%) coupled with

minor assimilation (≤9%) of dunite (0.5) and wehrlite (0.5) assemblages (Laiolo and Cigolini 2006).

Quite apart from its quantitative modeling, the difference observed between pre-paroxysm and post-paroxysm LP shards reflects different ascent rates and cooling rates and suggests that the pre-paroxysm LP shards may represent a small early volume of LP magma that traveled slower within the deep conduit with respect to later and larger volumes of fast-ascending LP magma erupted during the paroxysm. The small volume of LP magma and its slower ascent rate would also explain the unusual eruptive mechanism that produced repeated ash emissions instead of discrete Strombolian explosions, or violent paroxysmal eruption.

Lithium isotopic signatures of Recent Stromboli volcanics

A common Li isotope signature is shared by bulk pumices and lavas erupted in historical (360 BC to twentieth century AD) and recent (twentieth and twenty-first centuries AD) times and LP shards, and close similarity is also observed between δ^7Li values of LP magma and olivine-hosted melt inclusions (Schiavi 2007) (Fig. 6a). Lithium contents and isotopic compositions of LP shards and pumices fall inside the field which characterizes most of volcanic arc lavas (δ^7Li ~1–8‰, e.g. Moriguti and Nakamura 1998a; Chan et al. 2002b; Tomascak et al. 2002; Leeman et al. 2004; Moriguti et al. 2004; Magna et al. 2006; Halama et al. 2009) although they are mostly characterized by light lithium compositions. In addition, δ^7Li signature of LP shards and pumices overlap that of N-MORB ($\delta^7\text{Li} = +3.4 \pm 1.4$‰ ($2\sigma$), Chan et al. 1992, 2002a; Elliott et al. 2006; Tomascak et al. 2008). On the contrary, a wide spectrum of δ^7Li values is observed in HP glassy clasts that extend the field of isotopic compositions defined by LP magma and melt inclusions to lighter Li isotopic signatures. Since LP pumices and olivine-hosted melt inclusions represent the most primitive magmas erupted at Stromboli (Métrich et al. 2001; Bertagnini et al. 2003) and, hence the most suitable samples to preserve the Li isotopic composition of Stromboli magma sources, the wider δ^7Li variability and lighter Li compositions detected in HP shards are probably related to processes of ascent, ponding, and degassing along the crust. A possibility is that lighter δ^7Li values are either due to late processes (e.g., hydrothermal alteration) occurring within the plumbing system, most likely at shallow depth because the mass fractionation of lithium is strongest at low temperatures (<350°C, Chan et al. 1992, 2002a; Teng et al. 2004; Wunder et al. 2006), or are ruled by open system kinetic effects (e.g., Beck et al. 2004, 2006; Halama et al. 2007; Jeffcoate et al. 2007). Crystal fractionation is unlikely to lead to the large variation of δ^7Li observed in HP ashes (Tomascak et al. 1999b; Chan and Frey 2003; Jeffcoate et al. 2007). Isotopic composition of recently erupted magmas points against a significant role of crustal contamination on present-day Stromboli magmas (Francalanci et al. 1999, and references therein). Francalanci et al. (2005) proposed the existence of an older cumulus crystal mush zone below the Stromboli shallow reservoir, which is periodically disrupted and sampled by the ascending LP magma. However, our data show identical Li isotopic signatures for bulk pumices and lavas, thus suggesting that, if interaction of the HP magma with a cumulus crystal mush takes place, it does not produce appreciable effects on the δ^7Li signature of the shallow reservoir. Alternatively, it could be argued that the observed variation of Li isotopic ratios in HP shards is related to either kinetic fractionation during diffusion and/or degassing processes occurring at relatively shallow depth. The observed Li isotope fractionation cannot be accounted for by secondary alteration effects operated on the erupted ashes before their sampling by water-rich agents; indeed, secondary alteration would have affected in similar way both LP and HP shards and shifted original Li isotope ratios toward heavier compositions.

Degassing-induced fractional crystallization

There is general consensus that the Stromboli present-day activity is mostly ruled by steady arrival of primitive LP magma batches that progressively undergo decompression, lose gas, and possibly mix up with HP magma stalling in the upper plumbing system (Francalanci et al. 1999, 2004, 2005; Métrich et al. 2001; Bertagnini et al. 2003). As for the effects of Li isotopic fractionation induced by degassing, we explored this possibility by simulating the fractionation effects of an open-system Rayleigh distillation between melt and fluid phase (Fig. 6). In simulating an open-system Rayleigh distillation we used the formulation expressed as $\delta^7\text{Li} = ((\delta^7\text{Li})_0 + 1{,}000)f^{(\alpha-1)} - 1{,}000)$, in which δ^7Li and $(\delta^7\text{Li})_0$ represent Li isotopic compositions of the degassed and initial magma, respectively, f corresponds to the fraction of lithium remaining in the melt after degassing, and α is the Li isotope fractionation factor between vapor and melt, i.e. $(^7\text{Li}/^6\text{Li})_{\text{fluid}}/(^7\text{Li}/^6\text{Li})_{\text{melt}}$. If we assume that the original melt before significant degassing has the same composition of the post-paroxysm LP glass ($(\delta^7\text{Li})_0 = \sim+4$‰ and Li = 8 ppm ($C_0$)), then the Li isotopic composition of degassed melt as a function of f can be calculated provided that suitable values of α are known. Unfortunately, experimentally determined values of Li fractionation factor between vapor and melt under relevant conditions of pressure, temperature and melt composition are not currently available; in contrast, there is increasing experimental evidence on Li isotopic

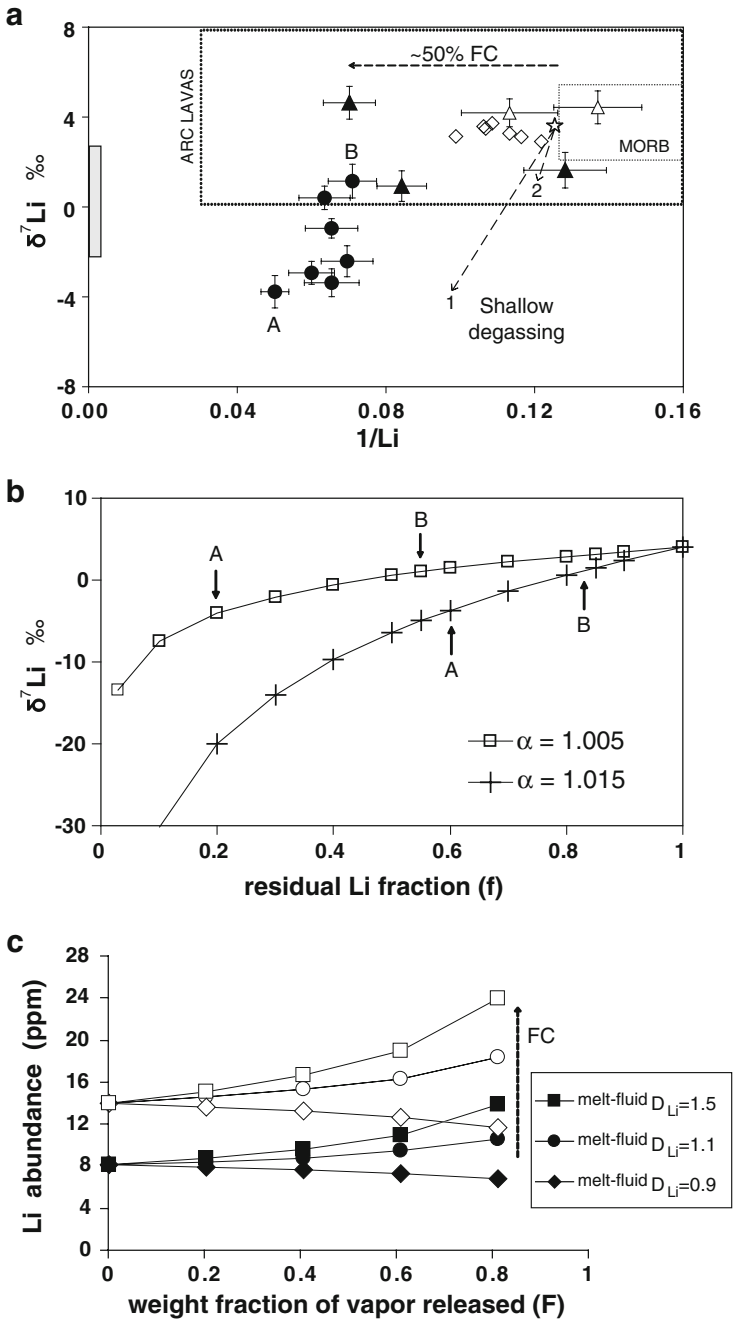

Fig. 6 **a** 1/Li versus δ^7Li plot for HP and LP glassy shards erupted in March–April 2003. *Error bars* represent 2σ. The bulk-rock compositions plotted for comparison (*open diamonds*; *error bars* smaller than *symbols*) include pumices (ST317, ST79p, ST81p and ST82p) and lava (ST010203, ST170503 and ST103) samples. The compositional fields for most of volcanic arc lavas and for N-MORB (see *references* in the text) are reported; the latter extends to higher 1/Li values. The *gray bar* drawn on the *y*-axis indicates the variation of Li isotopic composition preserved in olivine-hosted melt inclusions from pumice samples (Schiavi 2007). The *star* represents the average composition of the LP shards ejected in April (STR10-04-2003B), which is assumed as starting composition in the proposed model of degassing-induced crystallization. *A* and *B* are the HP fragments with the lightest and the heaviest Li isotopic signature, respectively, representing the end-members of the model. The *horizontal arrow* shows the range of variation for 1/Li when fractional crystallization approaches 50%; the *arrows* labeled with "*1*" and "*2*" indicate degassing trends. Compositions of *A* and *B* end-members are consistent with a vapor release of 40–50% (trend 1) and 10–20% (trend 2), respectively, if $^{melt/fluid}D_{Li} = 1.5$ and $\alpha = 1.015$ are assumed. By assuming $^{melt/fluid}D_{Li} = 1.1$ and $\alpha = 1.005$, *A* and *B* end-member compositions are consistent with ~80% (trend 1) and 35–45% (trend 2) of vapor release, respectively. **b** Fractionation paths of δ^7Li as function of residual Li fraction in the degassing HP magma, calculated for two different α values using the Rayleigh distillation equation (see *text* for explanation). *A* and *B* indicate the end-members of the degassing model shown in **a**. **c**. Variation of Li contents in HP melt as a function of the vapor fraction released during degassing (*solid symbols*) and associated fractional crystallization (~50%; *open symbols*). The trends for three different values of $^{melt/fluid}D_{Li}$ are shown

fractionation between fluid and mineral (Wunder et al. 2006, 2007). Beck et al. (2004) estimated the isotopic fractionation factor for Li_2O and Li_2S between vapor and melt lower than unity (0.966 and 0.978, respectively). However, these authors pointed out the importance of Li speciation (elemental Li, oxide Li_2O, chloride LiCl or sulfide Li_2S gas species) during migration from magma to gaseous phase in the determination of the α between fluid and melt. On this ground and in the absence of direct experimental evidence for Li fractionation between vapor and silicate melt, we assumed that fluids are enriched in ^{7}Li relative to silicates, as also supported by recent experimental evidence for spodumene-fluid and mica-fluid systems (Wunder et al. 2006, 2007). Experiments confirm theoretical prediction that Li fractionation factor $(^7Li/^6Li)_{fluid}/(^7Li/^6Li)_{mineral}$ increases with decreasing T (see Marschall et al. 2007, and references therein); α is 1.0024–1.0043 for T in the range 400–670°C, whereas it is in excess of 1.0056 and up to 1.015 for $T < 300$°C (see also Chan et al. 1992; Zack et al. 2003; Rudnick et al. 2004). Equilibrium temperature for quiescent degassing at Stromboli is estimated to be in the order of 700°C (Allard et al. 2008), so that low α values could be predicted extrapolating results for silicate mineral and fluid pairs. However, it seems plausible that vapor degassing from melt favors an easier and faster ^{7}Li removal with respect to fluid release from minerals. We notice here that if α values at the lowest end of the range reported above are assumed (i.e., 1.0024), then Li must be almost completely removed into the vapor phase to significantly change its isotopic composition in the residual melt, a feature not observed even in the highly evolved melts. In contrast, α values >1.004 may result in significant Li isotopic fractionation also in the case of partial removal of Li from melt and are therefore regarded as more realistic. Calculations show that assuming α in the order of 1.005 the lightest (−3.8‰, in the following called end-member A) and the heaviest (+1.2‰, in the following called end-member B) Li compositions of HP shards can be achieved when f is about 0.2 and 0.55, respectively. For $\alpha = 1.015$ (i.e., in the case of extreme Li fractionation) Li compositions of A and B end-members are obtained for f equal to 0.6 and 0.83, respectively (Fig. 6b).

The residual Li contents in HP glass after degassing (f) can be calculated using the equation $C_{residual} = C_0(1 - F)^{(1/D-1)}$, in which $C_{residual}$ and C_0 are the weight concentrations of Li in the degassed and original melt, respectively, F is the weight fraction of vapor phase released from the original melt and D is the bulk distribution coefficient for Li between melt and vapor. Experimental data on partitioning behavior of lithium between basaltic melt and hydrous fluid, under relevant conditions of pressure, temperature and melt compositions, are absent. London et al. (1988) performed vapor-saturated experiments at 200 MPa with peraluminous granitic melts and found that Li preferentially partitions into the melt (vapor-melt partition coefficient of ~0.4) within a temperature interval of 650–775°C. Webster et al. (1989) studied Li partitioning between hydrous fluid and metaluminous rhyolitic melts at 800°C and observed that Li preferentially partitions into the hydrous fluid, especially at lower pressure (~50 MPa), and that at higher pressure (200–500 MPa) its partitioning is more dependent on temperature and fluid composition, in particular on chlorine content of fluids. According to these authors, D_{Li} between melt and fluid would change from 0.4 to 2.0 at 200 MPa. Noticeably, the observed positive correlation between δ^7Li and 1/Li, which in turn implies $C_{residual}/C_0 > 1$, can be only explained by $^{melt/fluid}D_{Li}$ values significantly higher than unity (Fig. 6c), in agreement with results from London et al. (1988). Given the uncertainty on this value, modeling results are shown in Fig. 6c for the values of $^{melt/fluid}D^{Li} = 1.5$, 1.1 and 0.9. In modeling the variations of Li abundance in the degassing HP melt, we must also take into account the effects of fractional crystallization. In particular, fractionation of mineral phases in the extent (~50%) and modal proportions estimated on the basis of major and trace elements drives Li content of the degassing magma to increase by a factor 1.7 (Fig. 6a, c).

Altogether, modeling results indicate that δ^7Li values and Li contents of the lightest (A) and heaviest (B) end members are consistent with a vapor release of 40–50% and 10–20%, respectively, if $^{melt/fluid}D_{Li} = 1.5$ and $\alpha = 1.015$; on the other side, $^{melt/fluid}D_{Li} = 1.1$ and $\alpha = 1.005$ produce the observed HP compositions by about 80% and 35–45% of vapor release, respectively. As a whole, the variability of δ^7Li values (−3.8 to +1.2) and Li contents (mostly, from 12 to 20 ppm) of HP glass can be accounted for by variable degrees of fluid release during degassing coupled with slightly variable degrees of prevailing plagioclase and clinopyroxene fractionation.

Lithium isotope fractionation by diffusion: a qualitative assessment

Alternatively, the observed variation of Li isotopic ratios in HP glass shards could be related to kinetic fractionation during diffusion between the more primitive LP magma and the HP one, which is expected to occur depending on the Li concentration gradient between the coexisting magma batches. Experimental evidence indicates that lithium has an extraordinary mobility in igneous systems when compared to a broad range of elements, and its diffusion-induced isotope fractionation is in the order of tens per mil (Richter et al. 2003). These authors estimated diffusion coefficient of Li to be 6×10^{-5} cm^2 s^{-1} in a

basaltic liquid with $SiO_2 = 50$ wt.% at 1,350°C. On this ground, it is possible that chemical diffusion between LP and HP magmas might result in the observed Li isotope fractionation because of the significantly higher diffusivity of ^{6}Li with respect to ^{7}Li (Richter et al. 2003). However, since diffusion is expected to proceed from the Li-enriched end-member to the Li-depleted one, i.e., from the highly crystallized HP to the LP magma, this process would yield a lighter Li isotopic composition in the LP magma contrarily to our observations. Therefore, this process is unlikely to explain the variations of Li isotopic ratio in HP ashes.

On the other hand, we cannot rule out that a diffusion mechanism from the HP magma could have partially affected the Li isotope composition of the pre-paroxysm LP magma (sample STR08-03-2003) and shifted it toward lighter δ^7Li and higher Li contents (e.g., fragment 20), with respect to post-paroxysm LP ashes. We need to consider that the efficiency of diffusion processes will strongly depend on exposure time, contact interface, and occurrence of mingling between the two magmas, which most likely were rather small or limited to the syn-eruptive ascent and thus unable to affect the composition of major elements and trace elements other than lithium. Mingling is not evident by microscope observation at the scale of the ash clast. Detailed δ^7Li profiles in glassy samples of coexisting LP and HP magmas (i.e., mingled pumice-scoria clasts) are required to quantitatively test this hypothesis.

In addition, the lack of correlation between Li abundances and isotopic ratios of pre-paroxysm LP shards and analogously variable δ^7Li values found in melt inclusions suggest that δ^7Li signature of pre-paroxysm LP shards is not the result of a diffusion mechanism only. Two possible explanations are: (1) heterogeneity of Stromboli magma sources, and (2) interaction between LP magma and cumulates or crystal mushes occurring upon ascent in the deep plumbing system.

In summary, the Li isotopic compositions of HP magma cannot be explained by diffusion processes between HP and LP magmas. However, we agree that a more quantitative assessment of diffusion effects requires further Li profiles at the interface between LP and HP magmas where the mingling is evident. In addition, we notice that our data seem to be not consistent with Li isotope fractionation driven by diffusion between mineral phases, especially plagioclase, and HP melt. Indeed, in light of the significantly higher diffusivity of ^{6}Li with respect to ^{7}Li (Richter et al. 2003) and lower Li contents in plagioclase relative to the basaltic melt, the occurrence of diffusion processes should lead HP melts to evolve to isotopically heavier δ^7Li values (with respect to less differentiated LP melt) due to the faster diffusion of ^{6}Li into crystals, in disagreement with our observations. In contrast, available data and their modeling show that degassing coupled with fractional crystallization is a suitable and likely process to explain the compositional range of brown HP shards.

The 2003 eruptive scenario

Primitive magma ejected during paroxysms represents perturbations to the steady state of the magmatic feeding system of the ordinary Strombolian activity due to its faster ascent and, possibly, larger volumes than usual. In this context April 5 paroxysm is related to the arrival of a batch of primitive magma that underwent only minor fractional crystallization of mafic phases; a similar batch was collected as LP ash shards a few days later (Fig. 7). The distinct chemical signatures of LP and HP glass shards are thus related to the residence time within the plumbing system and to the different rate of volatile loss and fractional crystallization they underwent during the ascent. In contrast, the difference in the trace element fingerprinting of pre- and post-paroxysm LP products is negligible and reflects only slightly variable degrees of wall-rock assimilation and crystal fractionation between LP magma batches. These results confirm the overall scenario envisaged for the Stromboli 2003 eruptive activity (Métrich et al. 2001; Bertagnini et al. 2003; Francalanci et al. 2004; Landi et al. 2006). In addition, the investigation carried out on juvenile ashes reveals that small volumes of LP magma, slightly more differentiated than later pulses, ascended during the pre-paroxysm phase through the shallow plumbing system of the volcano and along the conduit and were emitted as blonde vesicular glassy shards (Fig. 7). These LP blobs behaved as a herald of the arrival of a larger volume of LP magma that was erupted during the April 5 paroxysm. It is noteworthy that, due to their small volume, these LP drops crossed the stationing HP magma body and arrived to the surface without a significant interaction, probably associated with small bubble plumes. For this reason they were not detected by the geophysical networks and overlooked by petrologic monitoring (Landi et al. 2006). Conversely, geochemical monitoring evidenced a marked increase of CO_2, H_2, and He dissolved in thermal waters and changes in the dissolved carbon isotopic composition (Carapezza et al. 2004) together with an increase of SO_2/HCl ratio in gas plume (Aiuppa and Federico 2004), few days before the paroxysm. Both geochemical anomalies have been interpreted as produced by depressurization of a rising batch of a deep gas-rich magma.

Two major points are worth discussing, namely the degassing mechanisms associated with HP and LP magmas and the significance of the different Sr isotopic signatures of these magma types (Francalanci et al. 1999, 2005).

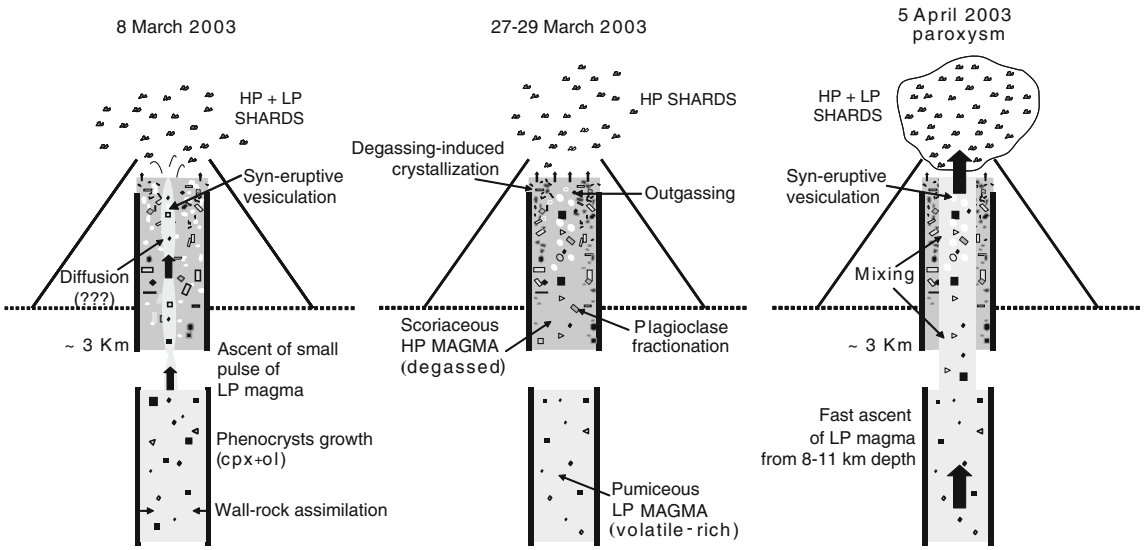

Fig. 7 The cartoon portrays a simplified model (not to scale) for Stromboli March–April 2003 activity and the relationships between HP (*dark gray*) and LP (*light gray*) magmas. On March 8, a small pulse of volatile-rich LP magma fractionating mafic phases and interacting with the wall-rock at depth ascended the conduit through HP magma residing at shallow levels. Both LP and HP shards were emitted. During the pre-paroxysm phase following March 8, the normal activity continued with HP magma undergoing continuous degassing and convection that enhance crystallization and zoning of plagioclase phenocrysts. Only HP brown shards were emitted. On April 5, a sudden pulse of more primitive volatile-rich magma, or decompression from the top, allowed the LP magma to rise up vigorously from about 8–11 km depth to the shallow portion of the plumbing system. This fast ascent promoted syn-eruptive volatile exsolution and was accompanied by reaction and mixing with the overlying degassed HP magma

Apparently, the similarly final low water content measured in residual melts of both magma types argues against the scenario envisaged here and particularly the proposed model of degassing-induced Li fractionation. The low water content of LP shards suggests that they also underwent strong degassing, in accordance with the rapid kinetics of vesiculation in basaltic magma; thus one could expect a shift toward lighter Li isotopic compositions in LP ashes as observed for HP analogs. However, it must be noticed that mechanisms of volatile exsolution, separation from the melt, and outgassing are significantly different for the two magma types (Polacci et al. 2006, and references therein). HP magma has longer residence times within the shallow level plumbing system ($P < 50$ MPa; Francalanci et al. 2004; Landi et al. 2004; Di Carlo et al. 2006). Under these conditions, HP magma undergoes relatively slow, non-explosive, and extremely efficient (open-system) degassing through a permeable network further enhanced by some magma overturn and convection (Burton et al. 2007; Lautze and Houghton 2007), which would facilitate the isotopic fractionation of lithium. In contrast, the faster ascent rates of LP magmas and their short or negligible residence at shallow level, when compared to HP magma, inhibit volatile-loss-induced crystal nucleation and result in syn-eruptive, fast degassing of H_2O. This process is probably unable to significantly fractionate Li isotopes since the LP magma behaves as a closed system until the arrival to the surface and equilibrates continuously with the vapor producing a more homogeneous isotopic signature.

The second point concerns strontium isotopic composition. The different Sr isotopic signatures of LP ($^{87}Sr/^{86}Sr \sim 0.70610$) and HP magmas ($^{87}Sr/^{86}Sr$ ranging from 0.70627 to 0.70615) may suggest that two different sources feed the present-day Stromboli activity (Francalanci et al. 2005). However, the whole data set presented here supports the view that the two magmas can form from a common parental melt, provided that the chemical effects of fractionation and degassing processes at different depth are taken into account. Detailed geochemical investigations of olivine-hosted melt inclusions also support this view (Métrich et al. 2001; Bertagnini et al. 2003). Moreover, preliminary Pb isotope data on the HP and LP shards and on melt inclusions from Recent Stromboli activity do not evidence distinct populations (Schiavi 2007). On this ground, the apparent decoupling between Li and Sr isotopic signatures most probably results from the different time scale of sampling. In the present work we focused on a short period of an eruption where feeding is dominated by a single source, while Sr isotope variation is documented in samples erupted in a time scale of decades. In other words, if at least two sources produced LP magmas in the past 2 ky, then it seems plausible that the residence time of HP magma within the shallow plumbing system is so long that this magma still records in crystals (that form more than

50% of the rocks) or crystal clots or wall cumulates the isotopic signatures of an old LP magma source.

An alternative and intriguing hypothesis, at present unconstrained, is that chemical diffusion and/or degassing processes may also rule small differences in Sr isotopic composition, as discussed for lithium. Conventionally measured $^{87}Sr/^{86}Sr$ values cannot detect the effects of Sr mass fractionation and a specific study should be designed to test the hypothesis. Unfortunately, experimental data on degassing-induced Sr fractionation and computational data by ab initio methods to thoroughly address this point are also lacking. We only notice here that although the diffused Li is far more isotopically fractionated in silicate liquids relative to Sr (Richter et al. 2003), diffusion-induced isotopic fractionation of Sr between two liquids driven by a concentration ratio similar to that observed between LP and HP ($\sim 0.3 \div 0.5$) could be roughly estimated in the order of few fractions per mil, if a β kinetic fractionation parameter similar to that of Ca is adopted (~ 0.075, Richter et al. 2003).

Concluding remarks

The chemical investigation of juvenile glassy fragments of ashes erupted from Stromboli during March and April 2003 has provided useful information in tracking magma processes at shallow depths. The well-known presence of two different kinds of products in Recent Stromboli ejects, namely HP and LP magmas, related to distinct ascent dynamics has been confirmed by our study of glass shards. Morphology and major and trace element chemistry concur to clearly distinguish within juvenile ashes the presence of two different glassy clasts formed by quenching of the two HP and LP magmas that coexist at different depths within the plumbing system.

The results of the present study argue in favor of a common origin for HP and LP melts; major and trace element composition of glass shards indicates that the primitive, volatile-bearing LP magma evolves after ponding in the upper level conduit by degassing-induced crystallization ($\sim 50\%$ of prevalent plagioclase and minor clinopyroxene and olivine) towards a volatile-poor, residual melt represented by the glass of HP products. The role of degassing-induced crystallization operating in the HP magma during its relatively long residence at shallow depth is highlighted by variations of Li abundances and isotopic signatures that can be reconciled with variable degrees of efficient open-system degassing. In contrast, chemical composition and Li isotopic signature of LP shards reflect the faster ascent rates of LP magma batches, and their short or negligible residence at shallow level, when compared to HP magma.

Finally, we remark that consistent insights on magma evolution and eruption dynamics of present Stromboli are derived from both studies of olivine-hosted melt inclusions (Métrich et al. 2001; Bertagnini et al. 2003) and chemical investigations of juvenile glassy ashes. The latter allowed to recognize for the first time the early ascent of small volume, undegassed and deep seated magma blobs before a violent paroxysm. In turn, this confirms that in situ petrological and geochemical investigations of juvenile ashes are a powerful tool in monitoring the volcanic activity and forecasting paroxysmal events (Schiavi et al. 2006).

Acknowledgments The authors are greatly indebted to A. Bertagnini, L. Francalanci, P. Landi, N. Métrich, M. Palenzona, C. Sakaguchi, R. Tanaka, S. Tommasini and A. Zanetti for providing samples, lab assistance, petrologic and chemical data and scientific advice. FS and RV wish to thank COE-21 (Japan) and the scientific and administrative staff of ISEI for giving the opportunity to conduct research in the PML lab, for providing assistance, as well as for their warm hospitality, during stages at Misasa. R. Halama, L. Francalanci and an anonymous reviewer are gratefully acknowledged for constructive criticism and comments that greatly improved an early version of the manuscript. This research was supported by COE-21 (Japan) and MIUR, CNR, INGV (Italy) funds.

References

Aiuppa A, Federico C (2004) Anomalous magmatic degassing prior to the 5th April 2003 paroxysm on Stromboli. Geophys Res Lett 31:L14607. doi:10.1029/2004GL020458

Allard P, Aiuppa A, Burton M, Caltabiano T, Federico C, Salerno G, La Spina A (2008) Crater gas emissions and the magma feeding system of Stromboli volcano. In: Calvari S, Inguaggiato S, Puglisi G, Ripepe M, Rosi M (eds) The Stromboli volcano. An integrated study of the 2002–2003 eruption. Geophysical monograph series 182, American Geophysical Union, pp 65–80

Andronico D, Corsaro RA, Cristaldi A, Polacci M (2009) Characterizing high energy explosive eruptions at Stromboli volcano using multidisciplinary data: an example from the 9 January 2005 explosion. J Volcanol Geotherm Res 176(4):541–550

Beck P, Barrat JA, Chaussidon M, Gillet PH, Bohn M (2004) Li isotopic variations in single pyroxenes from the Northwest Africa 480 shergottite (NWA 480): a record of degassing of Martian magmas? Geochim Cosmochim Acta 68:2925–2933

Beck P, Chaussidon M, Barrat JA, Gillet PH, Bohn M (2006) Diffusion induced Li isotopic fractionation during the cooling of magmatic rocks: the case of pyroxene phenocrysts from nakhlite meteorites. Geochim Cosmochim Acta 70:4813–4825. doi:10.1016/j.gca.2006.07.025

Berlo K, Blundy J, Turner S, Cashman K, Hawkesworth C, Black S (2004) Geochemical precursors to volcanic activity at Mount St. Helens, USA. Science 306:1167–1169. doi:10.1126/science.1103869

Bertagnini A, Coltelli M, Landi P, Pompilio M, Rosi M (1999) Violent explosions yield new insights into dynamic of Stromboli volcano. EOS Trans AGU 80(52):633–636

Bertagnini A, Métrich N, Landi P, Rosi M (2003) Stromboli volcano (Aeolian Archipelago, Italy): an open window on the deep-feeding system of a steady state basaltic volcano. J Geophys Res 108(B7). doi:10.1029/2002JB002146

Bertagnini A, Métrich N, Francalanci L, Landi P, Tommasini S, Conticelli S (2008) Volcanology and magma geochemistry of the present-day activity: constraints on the feeding system. In: Calvari S et al. (eds) The Stromboli volcano: an integrated study of the 2002–2003 eruption. AGU, Geophysical Monograph Series, vol 182, pp 19–37

Bindeman IN, Davis AM, Drake MJ (1998) Ion microprobe study of plagioclase-basalt partition experiments at natural concentrations levels of trace elements. Geochim Cosmochim Acta 62:1175–1193

Blundy J, Cashman K, Humphreys M (2006) Magma heating by decompression-driven crystallization beneath andesite volcanoes. Nature 443:76–80. doi:10.1038/nature05100

Brenan JM, Neroda CC, Lundstrom HF, Shaw FJ, Ryerson FJ, Phinney DL (1998) Behaviour of boron, beryllium and lithium during melting and crystallization: constraints from mineral-melt partitioning experiments. Geochim Cosmochim Acta 62:2129–2141

Burton MR, Mader HM, Polacci M (2007) The role of gas percolation in quiescent degassing of persistently active basaltic volcanoes. Earth Planet Sci Lett 264:46–60. doi:10-1016/j.epsl.2007.08.028

Carapezza ML, Inguaggiato S, Brusca L, Longo M (2004) Geochemical precursors of the activity of an openconduit volcano: the Stromboli 2002–2003 eruptive events. Geophys Res Lett 31. doi:10.1029/2004GL019614

Cashman KV (1992) Groundmass crystallization of Mount St. Helens dacite, 1980–1986: a tool for interpreting shallow magmatic processes. Contrib Mineral Petrol 109:431–449

Cashman KV, Hoblitt RP (2004) Magmatic precursors to the 18 May 1980 eruption of Mount St. Helens, USA. Geology 32:141–144. doi:10.1130/G20078.1

Chan LH, Frey FA (2003) Lithium isotope geochemistry of the Hawaiian plume: results from the Hawaiian scientific drilling project and Koolau volcano. Geochem Geophys Geosystems 4. doi:10.1029/2002GC000365

Chan LH, Edmond JM, Thompson G, Gillis K (1992) Lithium isotopic composition of submarine basalts—implications for the lithium cycle in the oceans. Earth Planet Sci Lett 108:151–160

Chan LH, Alt JC, Teagle DA (2002a) Lithium and lithium isotope profiles through the upper oceanic crust: a study of seawater-basalt exchange at ODP Sites 504B and 896A. Earth Planet Sci Lett 201:187–201

Chan LH, Leeman WP, You C-F (2002b) Lithium isotopic composition of Central American volcanic arc lavas: implications for modification of subarc mantle by slab-derived fluids: correction. Chem Geol 182:293–300

Corsaro RA, Pompilio M (2004) Magma dynamics in the shallow plumbing system of Mt. Etna as recorded by compositional variations in volcanics of recent summit activity (1995–1999). J Volcanol Geotherm Res 137(1–3):55–71

Couch S, Sparks RS, Carroll MR (2003) The kinetics of degassing-induced crystallization at Soufriere Hills Volcano, Montserrat. J Petrol 44:1477–1502

D'Orazio M, Armienti P, Cerretini S (1998) Phenocryst/matrix trace-element partition coefficients for hawaiite-trachyte lavas from the Ellittico volcanic sequence (Mt. Etna, Sicily, Italy). Mineral Petrol 64:65–88

DePaolo DJ (1981) Trace element and isotopic effects of combined wall-rock assimilation and fractional crystallization. Earth Planet Sci Lett 53:189–202

Di Carlo I, Pichavant M, Rotolo S, Scaillet B (2006) Experimental crystallization of a high-K arc basalt: the Golden Pumice, Stromboli volcano (Italy). J Petrol 47:1317–1343. doi:10.1093/petrology/eg1011

Di Roberto A, Bertagnini A, Pompilio M, Gamberi F, Marani MP, Rosi AM (2008) Newly discovered submarine flank eruption at Stromboli volcano (Aeolian Islands, Italy). Geophys Res Lett 35. doi:10.1029/2008GL034824

Duke JM (1976) Distribution of the period four transition elements among olivine, calcic clinopyroxene and mafic silicate liquid: experimental results. J Petrol 17:499–521

Elliott T, Jeffcoate A, Bouman C (2004) The terrestrial Li isotope cycle: light-weight constraints on mantle convection. Earth Planet Sci Lett 220:231–245. doi:10.1016/S0012-821X(04)00096-2

Elliott T, Thomas A, Jeffcoate A, Niu Y (2006) Lithium isotope evidence for subduction-enriched mantle in the source of mid-ocean-ridge basalts. Nature 443:565–568. doi:10.1038/nature05144

Francalanci L, Manetti P, Peccerillo A (1989) Volcanological and magmatological evolution of Stromboli volcano (Aeolian Islands): the roles of fractional crystallization, magma mixing, crustal contamination and source heterogeneity. Bull Volcanol 51:355–378

Francalanci L, Tommasini S, Conticelli S, Davies GR (1999) Sr isotope evidence for short magma residence time for the 20th century activity at Stromboli volcano, Italy. Earth Planet Sci Lett 167:61–69

Francalanci L, Tommasini S, Conticelli S (2004) The volcanic activity of Stromboli in the 1906–1998 AD period: mineralogical, geochemical and isotope data relevant to the understanding of the plumbing system. J Volcanol Geotherm Res 131:179–211. doi:10.1016/S0377-0273(03)00362-7

Francalanci L, Davies GR, Lustenhouwer W, Tommasini S, Mason P, Conticelli S (2005) Intra-grain Sr isotope evidence for crystal recycling and multiple magma reservoirs in the recent activity of Stromboli Volcano, Southern Italy. J Petrol 46(10):1997–2021. doi:10-1093/petrology/egi045

Francalanci L, Bertagnini A, Métrich N, Renzulli A, Vannucci R, Landi P, Del Moro S, Menna M, Petrone CM, Nardini I (2008) Mineralogical, geochemical, and isotopic characteristics of the ejecta from the 5 April, 2003 paroxysm at Stromboli, Italy: inferences on the preeruptive magma dynamics. In: Calvari S et al. (eds) The Stromboli Volcano: an integrated study of the 2002–2003 eruption. AGU, Geophysical Monograph Series, vol 182, pp 331–345

Gasparini C, Iannacone G, Scandone P, Scarpa R (1982) Seismotectonics of the Calabrian Arc. Tectonophysics 84:267–286

Gillot PY, Keller J (1993) Radiochronological dating of Stromboli. Acta Vulcanol 3:69–77

Guilbaud MN, Blake S, Thordarson T, Self S (2007) Role of syn-eruptive cooling and degassing on textures of lavas from the AD 1783–1784 Laki eruption, South Iceland. J Petrol 48:1265–1294. doi:10.1093/petrology/egm017

Halama R, McDonough WF, Rudnick RL, Keller J, Klaudius J (2007) The Li isotopic composition of Oldoinyo Lengai: nature of the mantle sources and lack of isotopic fractionation during carbonatite petrogenesis. Earth Planet Sci Lett 254:77–89

Halama R, Savov IP, Rudnick RL, McDonough WF (2009) Insights into Li and Li isotope cycling and sub-arc metasomatism from veined mantle xenoliths, Kamchatka. Contrib Mineral Petrol 158:197–222. doi:10.1007/s00410-009-0378-5

Hart SR, Dunn T (1993) Experimental cpx/melt partitioning of 24 trace elements. Contrib Mineral Petrol 113:1–8

Hornig-Kjarsgaard I, Keller J, Koberski U, Stadbauer E, Francalanci L, Lenhart R (1993) Geology, stratigraphy and volcanological evolution of the island of Stromboli, Aeolian Arc, Italy. Acta Vulcanol 3:21–68

James RH, Allen DE, Seyfried WE Jr (2003) An experimental study of alteration of oceanic crust and terrigenous sediments at moderate temperatures (51–350°C): insights as to chemical processes in near-shore ridge-flank hydrothermal systems. Geochim Cosmochim Acta 67:681–691

Jeffcoate AB, Elliott T, Kasemann SA, Ionov D, Cooper K, Brooker R (2007) Li isotope fractionation in peridotites and mafic melts. Geochim Cosmochim Acta 71:202–218. doi:10.1016/j.gca.2006.06.1611

Kobayashi K, Tanaka R, Moriguti T, Shimizu K, Nakamura E (2004) Lithium, boron and lead isotope systematics of glass inclusions in olivines from Hawaiian lavas: evidence for recycled components in the Hawaiian plume. Chem Geol 212:143–161. doi:10.1016/j.chemgeo.2004.08.050

Laiolo M, Cigolini C (2006) Mafic and ultramafic xenoliths in San Bartolo lava field: new insights on the ascent and storage of Stromboli magmas. Bull Volcanol 68:653–670. doi:10.1007/s00445-005-0040-7

Landi P, Métrich N, Bertagnini A, Rosi M (2004) Dynamics of magma mixing and degassing recorded in plagioclase at Stromboli (Aeolian Archipelago, Italy). Contrib Mineral Petrol 147:213–227. doi:10.1007/s00410-004-0555-5

Landi P, Francalanci L, Pompilio M, Rosi M, Corsaro RA, Petrone CM, Nardini I, Miraglia L (2006) The December 2002–July 2003 effusive event at Stromboli volcano, Italy: insights into the shallow plumbing system by petrochemical studies. J Volcanol Geotherm Res 155:263–284. doi:10.1016/j.jvolgeores.2006.03.032

Landi P, Métrich N, Bertagnini A, Rosi M (2008) Recycling and "rehydration" of degassed magma inducing transient dissolution/crystallization events at Stromboli (Italy). J Volcanol Geotherm Res 174(4):325–336

Landi P, Corsaro RA, Francalanci L, Civetta L, Miraglia L, Pompilio M, Tesoro R (2009) Magma dynamics during the 2007 Stromboli eruption (Aeolian Islands, Italy): mineralogical, geochemical and isotopic data. J Volcanol Geotherm Res (published on line). doi:10.1016/j.jvolgeores.2008.11.010

Lautze NC, Houghton BF (2007) Linking variable explosion style and magma textures during 2002 at Stromboli volcano, Italy. Bull Volcanol 69:445–460. doi:10.1007/s00445-006-0086-1

Leeman WP, Tonarini S, Chan LH, Borg LE (2004) Boron and lithium isotopic variations in a hot subduction zone—the southern Washington Cascades. Chem Geol 212(1–2):101–124. doi:10.1016/j.chemgeo.2004.08.010

London D, Hervig RL, Morgan GB (1988) Melt-vapor solubilities and elemental partitioning in peraluminous granite–pegmatite systems: experimental results with Macusani glass at 200 MPa. Contrib Mineral Petrol 99:360–373

Magna T, Wiechert U, Grove TL, Halliday AN (2006) Lithium isotope fractionation in the southern Cascadia subduction zone. Earth Planet Sci Lett 250:428–443. doi:10.1016/j.epsl.2006.08.019

Makishima A, Nakamura E (2006) Determination of major, minor and trace elements in silicate samples by ICP-QMS and ICP-SFMS applying isotope dilution-internal standardisation (ID-IS) and multi-stage internal standardisation. Geostand Geoanal Res 30:245–271

Marschall HR, Pogge von Strandmann PA, Seitz HM, Elliott T, Niu Y (2007) The lithium isotopic composition of orogenic eclogites and deep subducted slabs. Earth Planet Sci Lett 262:563–580. doi:10.1016/j.epsl.2007.08.005

Métrich N, Rutherford MJ (1998) Low pressure crystallization paths of H_2O-saturated basaltic-hawaiitic melts from Mt. Etna: implications for open-system degassing of basaltic volcanoes. Geochim Cosmochim Acta 62(7):1195–1205

Métrich N, Bertagnini A, Landi P, Rosi M (2001) Crystallization driven by decompression and water loss at Stromboli Volcano (Aeolian Islands, Italy). J Petrol 42(8):1471–1490

Métrich N, Bertagnini A, Landi P, Rosi M, Belhadj O (2005) Triggering mechanism at the origin of paroxysms at Stromboli (Aeolian Archipelago, Italy): the 5 April 2003 eruption. Geophys Res Lett 32. doi: 10.1029/2004GL022257

Moriguti T, Nakamura E (1998a) Across-arc variation of Li isotopes in lavas and implications for crust/mantle recycling at subduction zones. Earth Planet Sci Lett 163:167–174

Moriguti T, Nakamura E (1998b) High-yield lithium separation and the precise isotopic analysis for natural rock and aqueous samples. Chem Geol 145:91–104

Moriguti T, Shibata T, Nakamura E (2004) Lithium, boron and lead isotope and trace element systematics of Quaternary basaltic volcanic rocks in northeastern Japan: implications for variation of slab-derived fluid composition due to mineralogical reactions in the subducting slab. Chem Geol 212:81–100. doi:10.1016/j.chemgeo.2004.08.005

Nakamura E, Makishima A, Moriguti T, Kobayashi K, Sakaguchi C, Yokoyama T, Tanaka R, Kuritani T, Takei H (2003) Comprehensive geochemical analyses of small amounts (<100 mg) of extraterrestrial samples for the analytical competition related to the sample return mission MUSES-C. In: Kushiro I, Fujiwara A, Yano H (eds) Asteroidal sample preliminary examination team, inst space and astron sci report, sp no. 16. Sagamihara, Japan, pp 49–101

Noguchi S, Toramaru A, Shimano T (2006) Crystallization of microlites and degassing during magma ascent: constraints on the fluid mechanical behavior of magma during the Tenjo Eruption on Kozu Island, Japan. Bull Volcanol 68:432–449. doi:10.1007/s00445-005-0019-4

Ottolini L, Bottazzi P, Zanetti A, Vannucci R (1995) Determination of hydrogen in silicates by secondary ion mass spectrometry. Analyst 120:1309–1313

Peccerillo A, Taylor SR (1976) Geochemistry of Eocene calc-alkaline volcanic rocks from Kastamorum area, Northern Turkey. Contrib Mineral Petrol 58:63–81

Pichavant M, Di Carlo I, Le Gac Y, Rotolo SG, Scaillet B (2009) Experimental constraints on the deep magma feeding system at Stromboli Volcano, Italy. J Petrol 50:601–624. doi:10.1093/petrology/egp014

Piochi M, Polacci M, De Astis G, Zanetti A, Mangiacapra A, Vannucci R, Giordano D (2008) Texture and composition of pumices and scoriae from the Campi Flegrei caldera (Italy): Implications on the dynamics of explosive eruptions. Geochem Geophys Geosyst 9. doi: 10.1029/2007GC001746

Polacci M, Baker DR, Mancini L, Tromba G, Zanini F (2006) Three-dimensional investigation of volcanic textures by X-ray microtomography and implications for conduit processes, Geophys Res Lett 33. doi:10.1029/2006GL026241

Puglisi G, Bonaccorso A, Mattia M, Aloisi M, Bonforte A, Campisi O, Cantarero M, Falzone G, Puglisi B, Rossi M (2005) New integrated geodetic monitoring system at Stromboli volcano (Italy). Eng Geol 79:13–31

Richter FM, Davis AM, De Paolo DJ, Watson EB (2003) Isotope fractionation by chemical diffusion between molten basalt and rhyolite. Geochim Cosmochim Acta 67:3905–3923

Ripepe M, Marchetti E, Ulivieri G, Harris A, Dehn J, Burton M, Caltabiano T, Salerno G (2005) Effusive to explosive transition during the 2003 eruption of Stromboli volcano. Geology 33:341–344. doi:10.1130/G21173.1

Rosi M, Bertagnini A, Landi P (2000) Onset of the persistent activity at Stromboli Volcano (Italy). Bull Volcanol 62:294–300. doi:10.1007/s004450000098

Rosi M, Bertagnini A, Harris A, Pioli L, Pistolesi M, Ripepe M (2006) A case history of paroxysmal explosion at Stromboli: timing and dynamics of the April 5, 2003 event. Earth Planet Sci Lett 243:594–606. doi:10.1016/j.epsl.2006.01.035

Rudnick RL, Tomascak PB, Njo HB, Gardner LR (2004) Extreme lithium isotopic fractionation during continental weathering revealed in saprolites from South Carolina. Chem Geol 212:45–57. doi:10.1016/j.chemgeo.2004.08.008

Ryan JG, Langmuir CH (1987) The systematics of lithium abundances in young volcanic rocks. Geochim Cosmochim Acta 51:1727–1741

Schiavi F (2007) Studio geochimico di inclusioni vetrose e ceneri nei prodotti dell′attivitá recente dei vulcani Stromboli ed Etna: implicazioni per l′origine e l′evoluzione dei magmi. Ph.D. Thesis, University of Pavia

Schiavi F, Tiepolo M, Pompilio M, Vannucci R (2006) Tracking magma dynamics by laser ablation (LA)-ICPMS trace element analysis of glass in volcanic ash: the 1995 activity of Mt. Etna. Geophys Res Lett 33(5). doi:10.1029/2005GL024789

Spadaro FR, Lefevre RA, Ausset P (2002) Experimental rapid alteration of basaltic glass: implications for the origins of atmospheric particulates. Geology 30(8):671–674

Speranza F, Pompilio M, Sagnotti L (2004) Paleomagnetism of spatter lavas from Stromboli volcano (Aeolian Islands, Italy): implications for the age of paroxysmal eruptions. Geophys Res Lett 31. doi:10.1029/2003GL018944

Speranza F, Pompilio M, D'Ajello Caracciolo F, Sagnotti L (2008) Holocene eruptive history of the Stromboli volcano: constraints from paleomagnetic dating. J Geophys Res 113. doi: 10.1029/2007JB005139

Sun SS, McDonough WF (1989) Chemical and isotopic systematics of oceanic basalts: implications for mantle composition and processes. In: Saunders AD, Norry MJ (eds) Magmatism in the Oceanic Basins. Geol Soc Spec Publ 42, pp 313–345

Tang YJ, Zhang HF, Nakamura E, Moriguti T, Kobayashi K, Ying JF (2007) Lithium isotopic systematics of peridotite xenoliths from Hannuoba, North China Craton: implications for melt-rock interaction in the considerably thinned lithospheric mantle. Geochim Cosmochim Acta 71:4327–4341. doi:10.1016/j.gca.2007.07.006

Teng FZ, McDonough WF, Rudnick RL, Dalpé C, Tomascak PB, Chappell BW, Gao S (2004) Lithium isotopic composition and concentration of the upper continental crust. Geochim Cosmochim Acta 68:4167–4178. doi:10.1016/j.gca.2004.03.031

Tepley FJ, Davidson JP, Tilling RI, Arth JG (2000) Magma mixing, recharge and eruption histories recorded in plagioclase phenocrysts from El Chichon Volcano, Mexico. J Petrol 41:1397–1411

Tiepolo M, Tribuzio R, Vannucci R (2002) The compositions of mantle-derived melts developed during the Alpine continental collision. Contrib Mineral Petrol 144:1–15. doi:10.1007/s00410-002-0387-0

Tiepolo M, Bottazzi P, Palenzona M, Vannucci R (2003) A laser probe coupled with ICP-double-focusing sector-field mass spectrometer for in situ analysis of geological samples and U–Pb dating of zircon. Can Mineral 41:259–272

Tomascak PB (2004) Developments in the understanding and application of lithium isotopes in the Earth and planetary sciences. In: Johnson C, Beard B, Albarede F (eds) Geochemistry of non-traditional stable isotopes. Minerological Society of America, Washington, pp 153–195

Tomascak PB, Carlson RW, Shirey SB (1999a) Accurate and precise determination of Li isotopic compositions by multicollector sector ICP-MS. Chem Geol 158:145–154

Tomascak PB, Tera F, Helz RT, Walker RJ (1999b) The absence of lithium isotope fractionation during basalt differentiation: new measurements by multicollector sector ICP-MS. Geochim Cosmochim Acta 63(6):907–910

Tomascak PB, Widom E, Benton LD, Goldstein SL, Ryan JG (2002) The control of lithium budgets in island arcs. Earth Planet Sci Lett 196:227–238

Tomascak PB, Langmuir CH, le Roux PJ, Shirey SB (2008) Lithium isotopes in global mid-ocean ridge basalts. Geochim Cosmochim Acta 72:1626–1637. doi:10.1016/j.gca.2007.12.021

Vaggelli G, Olmi F, Conticelli S (1999) Evaluation of analytical errors during microprobe analyses of silicate minerals international reference samples. Acta Volcanol 11:297–303

Watanabe Koichiro, Danhara T, Watanabe Kazunori, Terai K, Yamashita T (1999) Juvenile volcanic glass erupted before the appearance of the 1991 lava dome, Unzen volcano, Kyushu, Japan. J Volcanol Geotherm Res 89:113–121

Webster JD, Holloway JR, Hervig RL (1989) Partitioning of lithophile trace elements between H_2O and $H_2O + CO_2$ fluids and topaz rhyolite melt. Econ Geol 84:116–134. doi:10.2113/gsecongeo.84.1.116

Wolf KJ, Eichelberger JC (1997) Syneruptive mixing, degassing, and crystallization at Redoubt Volcano, eruption of December 1989–May 1990. J Volcanol Geotherm Res 75:19–37

Wunder B, Meixner A, Romer RL, Heinrich W (2006) Temperature-dependent isotopic fractionation of lithium between clinopyroxene and high-pressure hydrous fluids. Contrib Mineral Petrol 151:112–120. doi:10.1007/s00410-005-0049-0

Wunder B, Meixner A, Romer RL, Feenstra A, Schettler G, Heinrich W (2007) Lithium isotope fractionation between Li-bearing staurolite, Li-mica and aqueous fluids: an experimental study. Chem Geol 238:277–290

Yokoyama T, Makishima A, Nakamura E (1999) Evaluation of the coprecipitation of incompatible trace elements with fluoride during silicate rock dissolution by acid digestion. Chem Geol 157:175–187

Zack T, Tomascak PB, Rudnick RL, Dalpe C, McDonough WF (2003) Extremely light Li in orogenic eclogites: the role of isotope fractionation during dehydration in subducted oceanic crust. Earth Planet Sci Lett 208:279–290

Zanetti A, Tiepolo M, Oberti R, Vannucci R (2004) Trace-element partitioning in olivine: modeling of a complete data set from a synthetic hydrous basanite melt. Lithos 75:39–54